FINAL REPORT

Discrete Component Bonding and Thick Film Materials Study

Contract No. NAS8-30883

Period Covered: September 1, 1975 - September 30, 1976

Prepared for

George C. Marshall Space Flight Center
Marshall Space Flight Center, Alabama 35812

Prepared by

D. L. Kinser
Vanderbilt University
Department of Mechanical Engineering and Materials Science
Nashville, Tennessee 37235

Reported:

December 3, 1976

Abstract: The focus of this program has been twofold: first, the bonding reliability of discrete capacitor chips bonded with solders and conductive epoxies was examined and, second, the thick film resistor materials consisting of iron oxide phosphate and vanadium oxide phosphates were examined. The bonding reliability studies have concluded that none of the wide range of types of solders examined is capable of resisting failure during thermal cycling while the conductive epoxy gives substantially lower failure rates. The thick film resistor studies have proven the feasibility of iron oxide phosphate resistor systems although some environmental sensitivity problems remain. The vanadium oxide phosphate resistor system has shown promise, but the investigation is presently incomplete with respect to oxidation/reduction studies. One of these resistor compositions has inadvertently proven to be a candidate for thermistor applications because of the excellent control achieved upon the temperature coefficient of resistance. One new and potentially damaging phenomena uncovered observed was the degradation of thick film conductors during the course of thermal cycling.

TABLE OF CONTENTS

	Page
Abstract	ii
List of Figures	iv
Discrete Component Bonding Studies	1
Objective	1
Experimental Procedure	1
Experimental Results	3
Thick Film Resistor Material Studies	12
Vanadium Electrical Results	13
Summary of Present Program	16
Further Work	16
Appendix I	
"Reliability of Soldered Joints in Thermal Cycling Environments"	
Appendix II	
"Iron Phosphate Glass as a Thick Film Resistor Paste"	

LIST OF FIGURES

Figure		Page
1.	Cumulative failures as a function of number of thermal cycles for samples of 63 Sn 37 Pb quenched from the soldering temperature	4
2.	Cumulative failures as a function of number of thermal cycles for the 63 Sn 37 Pb quenched from the soldering temperatures. From previous report issued on work of 1974/75	4
3.	Cumulative failures as a function of number of thermal cycles for the 63 Sn 37 Pb slow cooled from the soldering temperature	5
4.	Cumulative failures as a function of number of thermal cycles of the 63 Sn 37 Pb slowly cooled from the soldering temperature. From previous report of work conducted during 1974/75	5
5.	Cumulative failures as a function of number of thermal cycles of the 97.5 Pb 1.5 Ag 1 Sn solder quenched from the soldering temperature	6
6.	Cumulative failures as a function of number of thermal cycles of the 97.5 Pb 1.5 Ag 1 Sn solder slowly cooled from the soldering temperature	6
7.	Cumulative failures as a function of number of thermal cycles of the Epotek H-44 gold-filled epoxy system	7
8.	A) Photograph of the thermal cycling test substrates as prepared 63 Sn 37 Pb quenched	9
	B) Photograph of the thermal cycling test substrates 63 Sn 37 Pb after 1000 cycles	9
	C) Photograph of the thermal cycling test substrates as prepared 97.5 Pb 1.5 Ag 1 Sn	10
	D) Photograph of the thermal cycling test substrates 97.5 Pb 1.5 Ag 1 Sn after 1000 cycles	10
	E) Photograph of the thermal cycling test substrates gold-filled epoxy after 1000 cycles	11

Figure Page

9. Resistance change as a function of temperature for the 70 V_2O_5- 30 P_2O_5 paste fired as noted 14

10. Resistance change as a function of specific power for the 70 V_2O_5- 30 P_2O_5 resistors fired as noted 14

DISCRETE COMPONENT BONDING STUDIES

Objective

This portion of the present program has focused upon the reliability of several types of bonding systems utilizing a ceramic chip capacitor as a typical discrete component. The bonding systems which have been examined include the conventional 63 Sn 37 Pb solder, a 96 Sn 4 Ag, a 97.5 Pb 1.5 Ag 1 Sn and the Epotek H-44 gold filled epoxy. The efficacy of each type bond was examined using a thermal cycling test according to MIL-STD-883A Method 1010.1 test condition B with exposure to 1000 cycles. The samples were examined during the course of the thermal cycling by measuring the capacitance of the system as well as by visual examinations.

Experimental Procedure

For purposes of the present experimental evaluation, the substrate chosen was American Lava type 614 with commercial surface finish. The conductor metallization was DuPont type 9596, and the solders chosen were manufactured by Kester with the compositions mentioned above. A Kester flux type 1544A was employed in all soldering operation. The capacitor chips employed were the Union Carbide Khemet 10^4 picofarad of 20% tolerance and 50 volt rating with a BX type dielectric. The capacitor terminations were supplied by UC in an untinned form to allow each solder type to be applied by a predip. The epoxy was applied to a chip from the same manufacturing lot but with a gold overcoat on the copper diffusion barrier employed by this vendor.

The capacitors were mounted on a specially designed metallization pattern which allowed 25 chips to be mounted on each substrate. The metallization was printed, dried and fired in accordance with the manufacturer's instructions. The 97.5 Pb 1.5 Ag 1 Sn* solder was especially aggressive at the soldering

*All solder designations are given in weight percent of each component.

temperatures and the metallization was rapidly removed during a pretinning operation. This forced the use of a copper electroplate over the metallization before the pretinning to avoid leaching of the metallization by the molten solder during pretinning. The substrates were pretinned by briefly dipping in the solder at the appropriate temperature depending upon the composition. The substrates were removed from the solder bath in a vertical orientation to promote drainage of solder from the substrate. The capacitors were then placed in the appropriate positions and the system was placed on a hotplate whose temperature was carefully controlled utilizing thermocouple measurements. Two cooling techniques were used as previously described in this work.* The complete soldered substrates were then cleaned using toluene and the soldered joints were visually inspected for cracks in solder joints, metallization and capacitor chips.

The epoxy bonded chips were prepared using a gold metallization, DuPont 9260 of the same pattern as that employed in the soldered systems. This conductor metallization was also processed in accordance with the manufacturer's recommendations. The epoxy, Epotek H-44, a gold-filled single component system was placed on the bonding pads of the substrate using a Laurier Associates epoxy dispenser and the gold-plated capacitor terminations were placed in position. The system was then subjected to 1/2 hour cure at 150°C as recommended by the epoxy manufacturer.

All the substrates were photographed after visual inspection at 0, 100, 200, 500 and 1000 cycles.

The thermal cycling in accordance with MIL-STD-883A was conducted using a Thermodynamic Engineering apparatus designed for thermal shock studies. This system was modified by the addition of a small copper container which effectively isolated the parts from the shock but allowed the parts to rapidly reach the test temperature. After thermal cycling, some of the parts were subjected

*See appended paper for detailed cooling rate discussion.

to destructive physical analysis in order to elucidate the cause of failure in the substrate-to-chip capacitor bonding sytem.

Experimental Results

The primary results of the bonding reliability studies are presented in Figures 1 through 7. Two of these results, Figures 2 and 4, are duplicates of work from last year's program which are included for comparison purposes. Figure 1 is the cumulative failure data for the 63 Sn 37 Pb solder conducted during the present year's program while Figure 2 is of a similar study conducted during 1974/1975. It is clear that these two results are quite similar and this bonding system results in failure rates in excess of 50% after 1000 thermal cycles. The experimental program thus appears to give reproducible results from samples processed approximately one year apart. Figures 3 and 4 represent the present and preceding year's work on the 63 Sn 37 Pb which was slowly cooled from the soldering temperature. The agreement between last year's results and the present result is rather poor in that failure rates in the present year's tests give failure rates substantially lower than previous results. The data 1000 cycles of the present year were unavailable because of the corrosion of the system which rendered electrical contact to the system metallization impossible. It can thus be assumed that 100% failure was observed in one of the two substrates examined. The corrosion phenomena was observed only in the present studies and appears to result in a green corrosion product which may be a copper cloride. No other substrates exhibited this phenomena and all were subjected to the same environment during simultaneous cycling.

Results for the 97.5 Pb 1.5 Ag 1 Sn are shown in Figure 5 for the quenched condition and Figure 6 for the slow cooled configuration. The results for the quenched and slow cooled samples appear to be quite similar although some

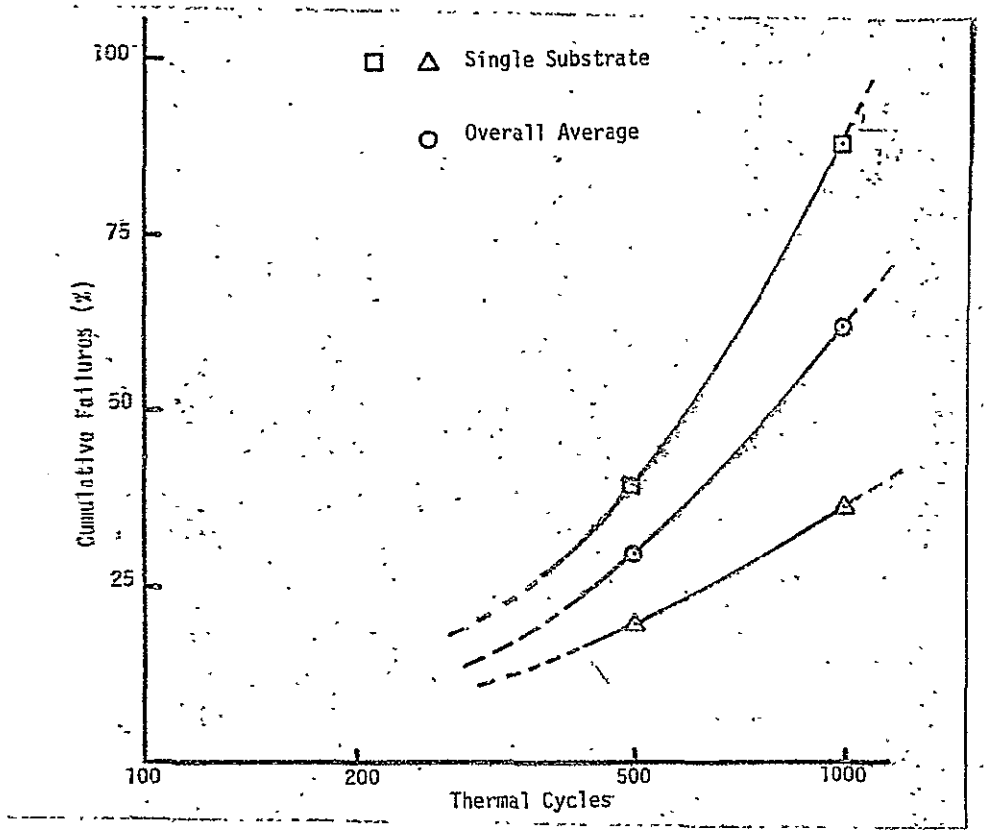

Figure 1. Cumulative failures as a function of number of thermal cycles for samples of 63 Sn 37 Pb quenched from the soldering temperature.

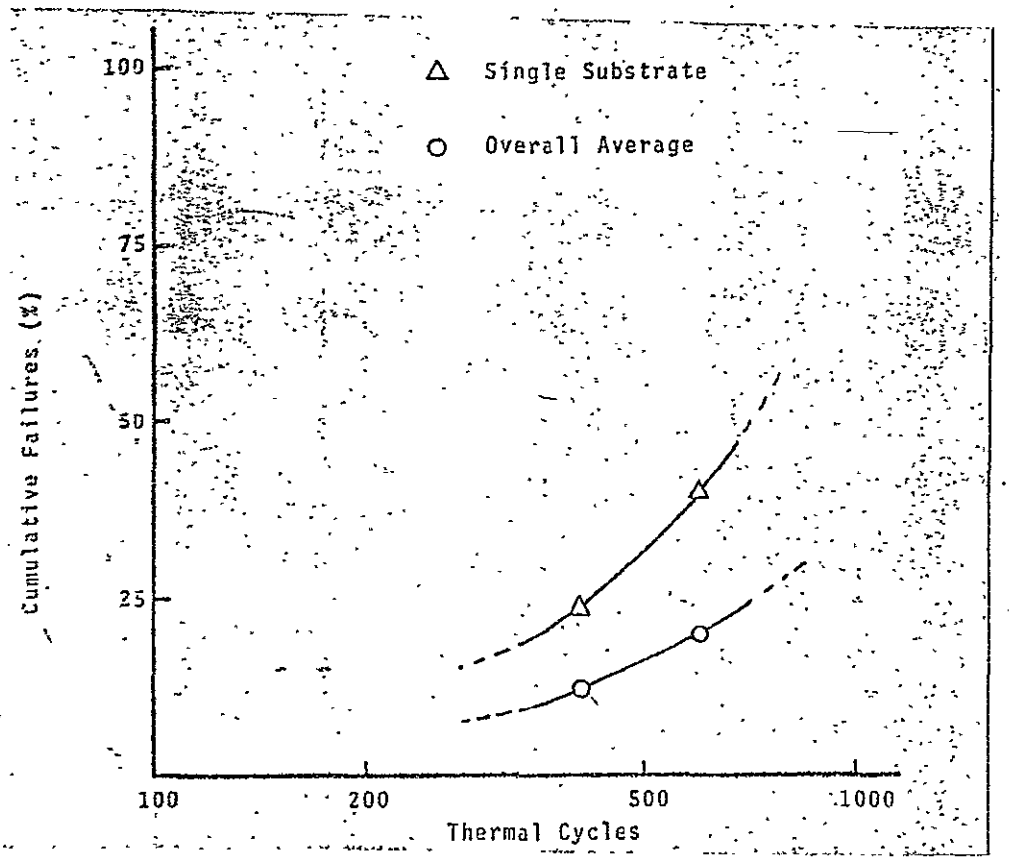

Figure 2. Cumulative failures as a function of number of thermal cycles for the 63 Sn 37 Pb quenched from the soldering temperature. From previous report issued on work of 1974/75.

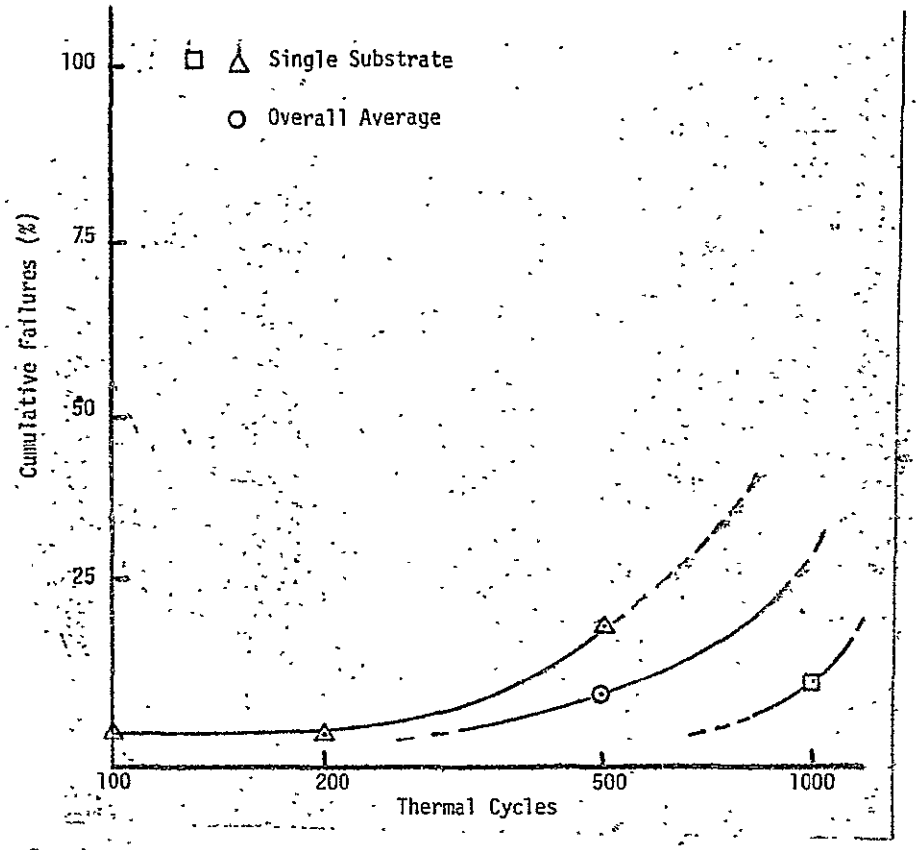

Figure 3: Cumulative failures as a function of number of thermal cycles for the 63 Sn 37 Pb slow cooled from the soldering temperature.

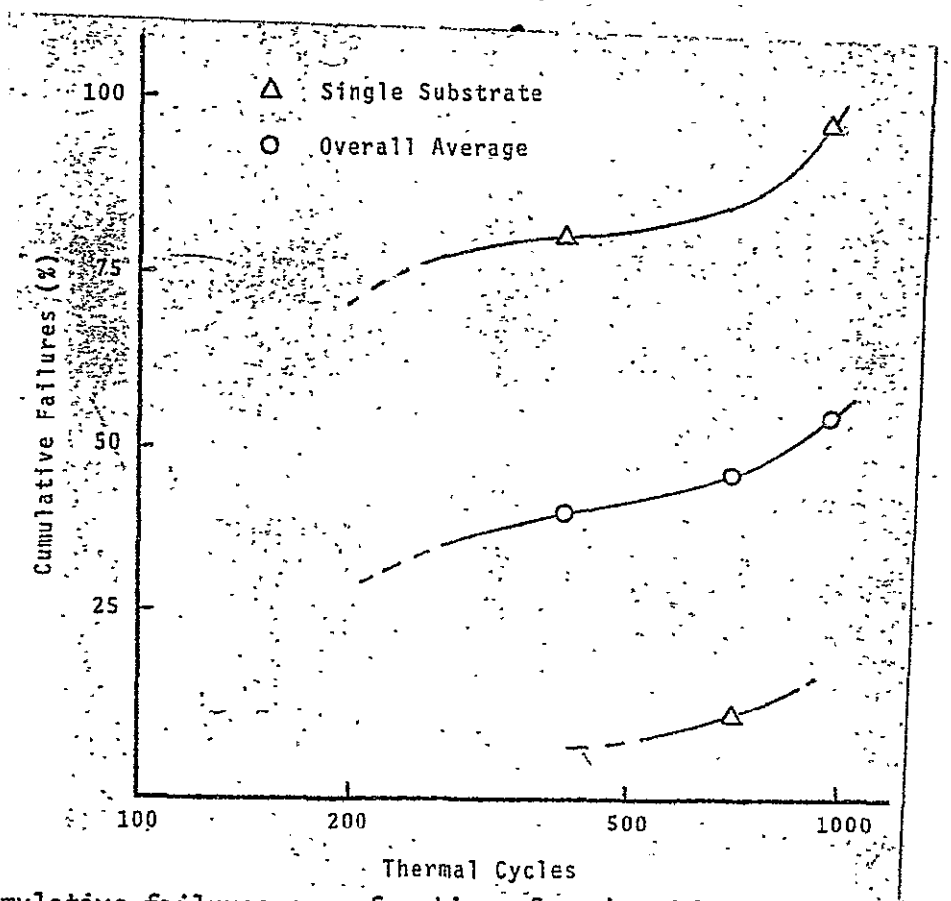

Figure 4. Cumulative failures as a function of number of thermal cycles of the 63 Sn 37 Pb slowly cooled from the soldering temperature. From previous report of work conducted during 1974/75.

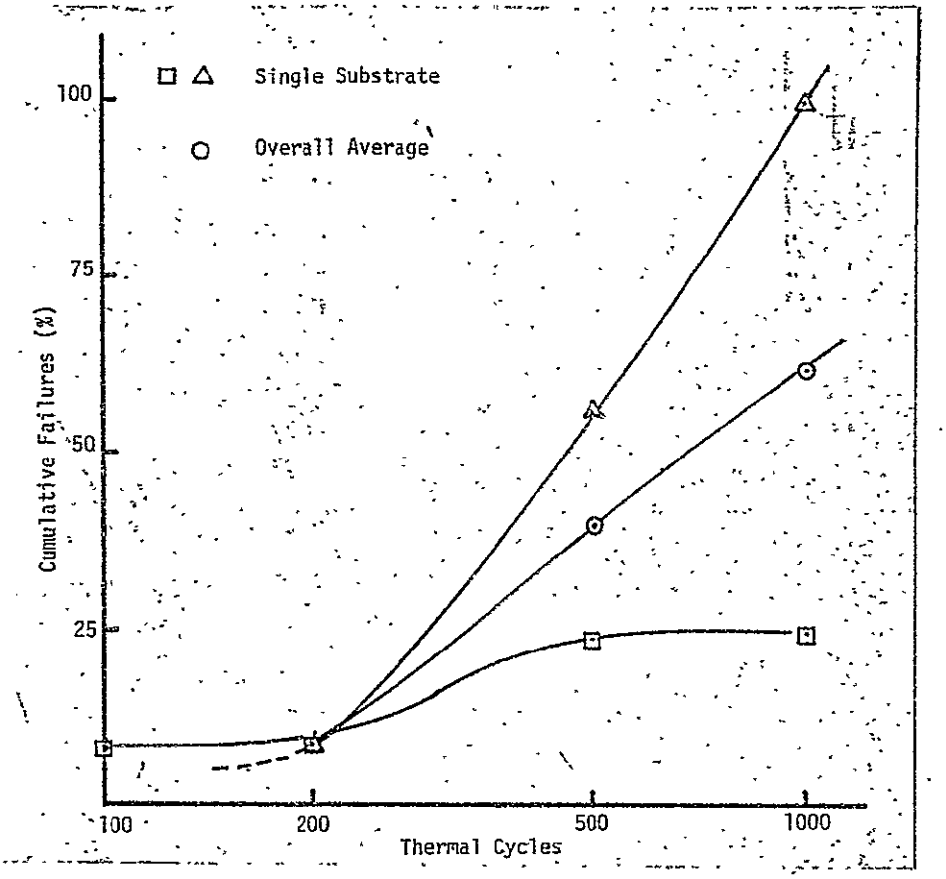

Figure 5. Cumulative failures as a function of number of thermal cycles of the 97.5 Pb 1.5 Ag 1 Sn solder quenched from the soldering temperature.

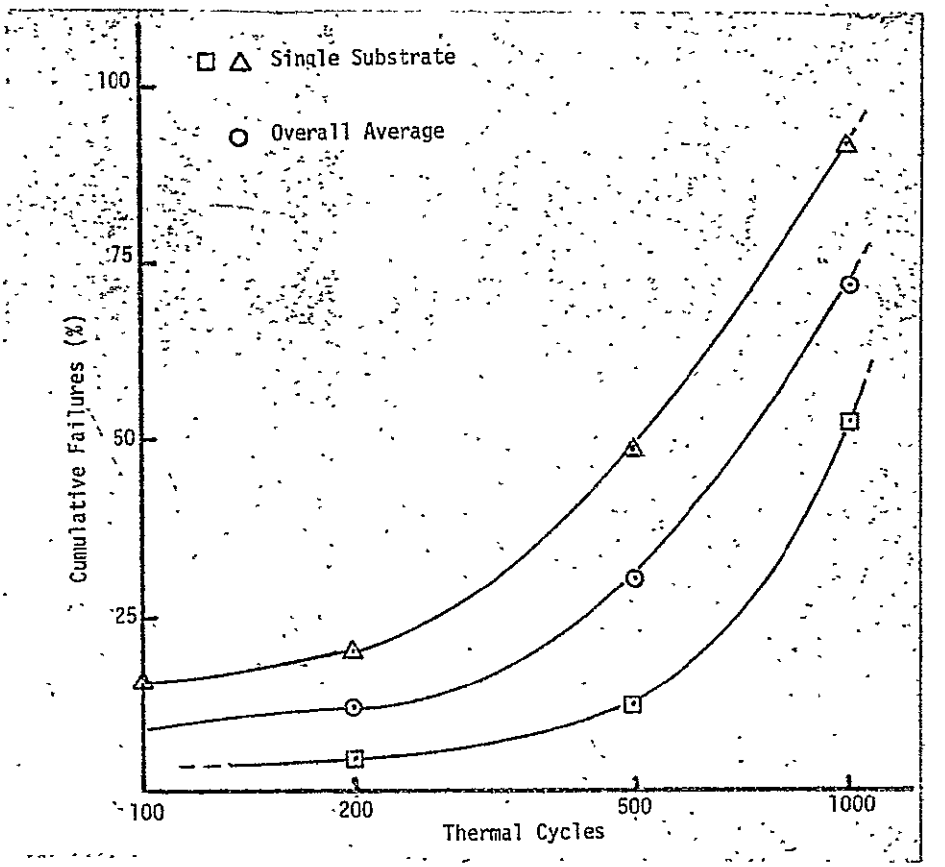

Figure 6. Cumulative failures as a function of number of thermal cycles of the 97.5 Pb 1.5 Ag 1 Sn solder slowly cooled from the soldering temperature.

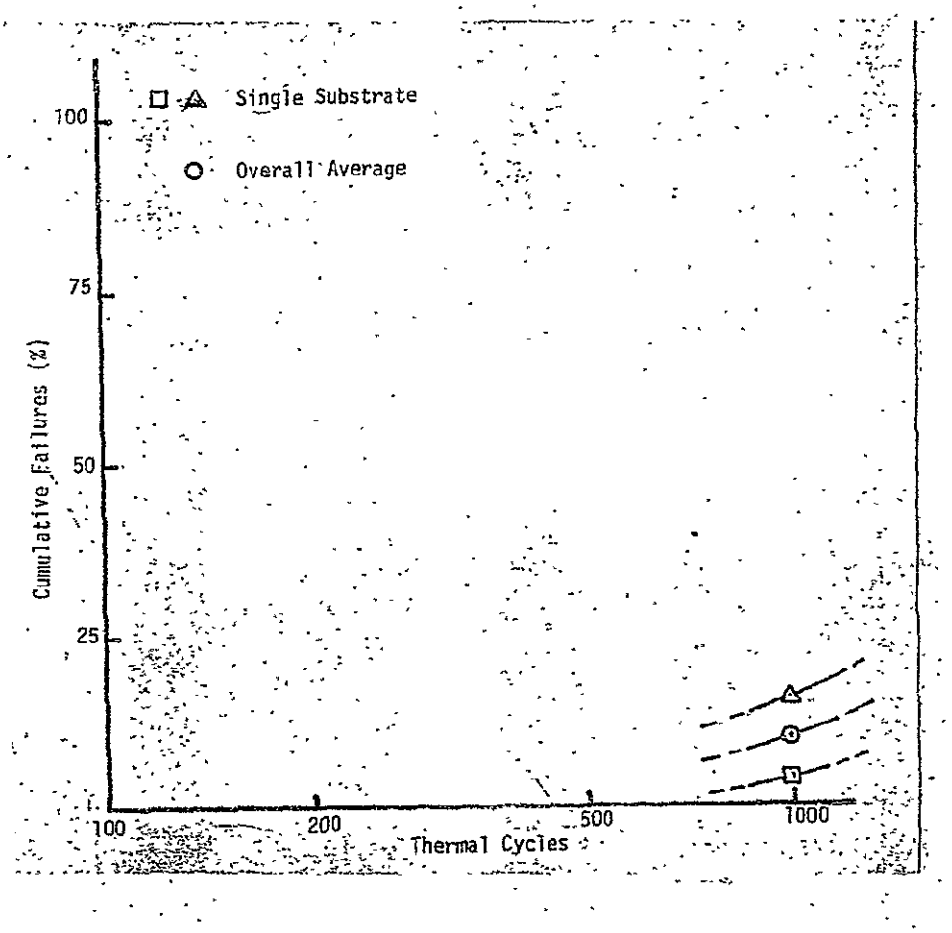

Figure 7. Cumulative failures as a function of number of thermal cycles of the Epotek H-44 gold-filled epoxy system.

statistical fluctuations are apparent. The overall failure behavior of this solder is quite similar to the conventional 63 Sn 37 Pb data reported in Figures 1 and 2. This system is, like the 63 Sn 37 Pb, not acceptable for systems where high reliability must be attained.

The results shown in Figure 6 for the epoxy bonded system (Epotek H-44 gold-filled) are substantially more promising than the solders mentioned above. The average cumulative percentage of failures at 1000 cycles for these systems is only 10% as contrasted with rates in excess of 50% for all solder systems examined.

The results of destructive physical analysis on the 63 Sn 37 Pb solder were presented at the International Microelectronics Conference held in Anaheim, California, in conjunction with the NEPCON 1976 Conference. The paper presented at this conference is attached and summarizes the results of the DPA. The fundamental conclusion of this report as well as the data presented above indicates that soldered joints of the types examined to this time show virtually no promise for use in high reliability military or aerospace applications.

This point is probably best made by reference to Figure 8 which is a compilation of photographs made during the present work. It is apparent from Figure 8A that the as prepared sample is of high quality and no visually rejectable solder joints or fillets were initially present. This same substrate shown in Figure 8B after 1000 cycles exhibits the degrading effects of thermal cycling which are typical of the 63 Sn 37 Pb solder system. The metallization is degraded and in some cases required repair to allow electrical testing of the capacitor/metallization bond. In all cases, the solder joint itself has lost its characteristic luster and taken on a chalky appearance. Figure 8C is of the as prepared 97.5 Pb 1.5 Ag 1 Sn solder system and, again, indicates the high quality appearance of

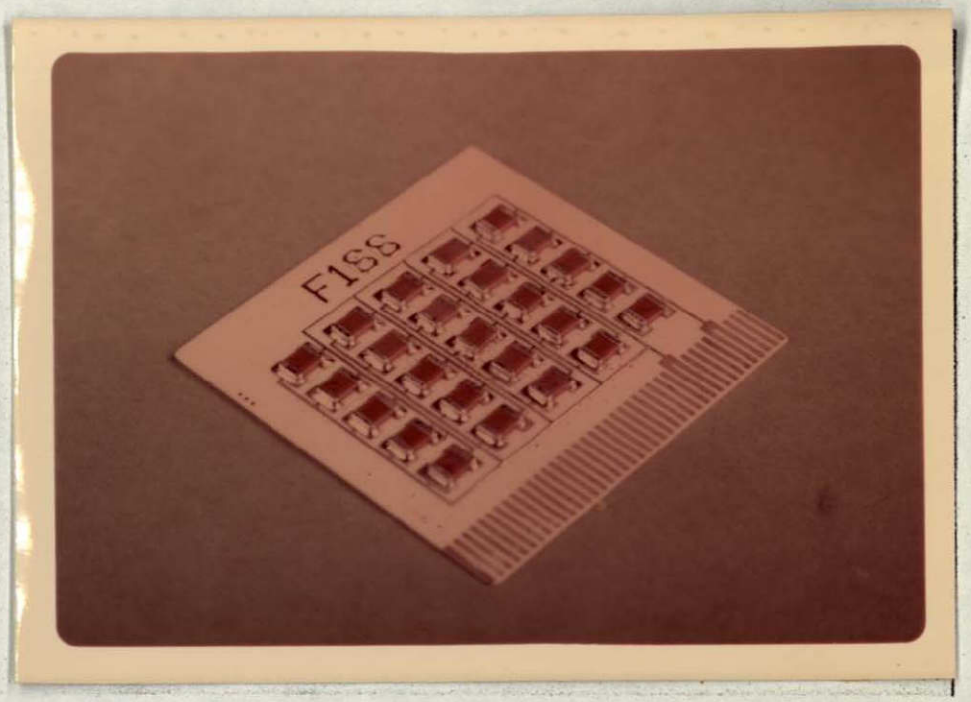

9

Figure 8A. Photograph of the thermal cycling test substrates as prepared 63 Sn 37 Pb quenched.

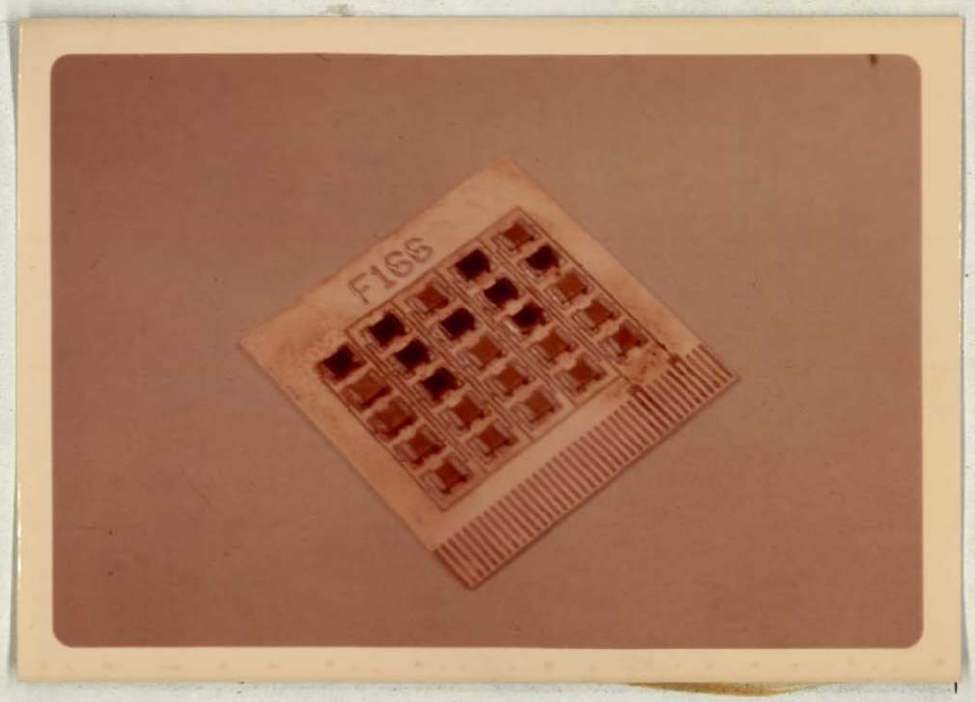

Figure 8B. Photograph of the thermal cycling test substrates 63 Sn 37 Pb after 1000 cycles.

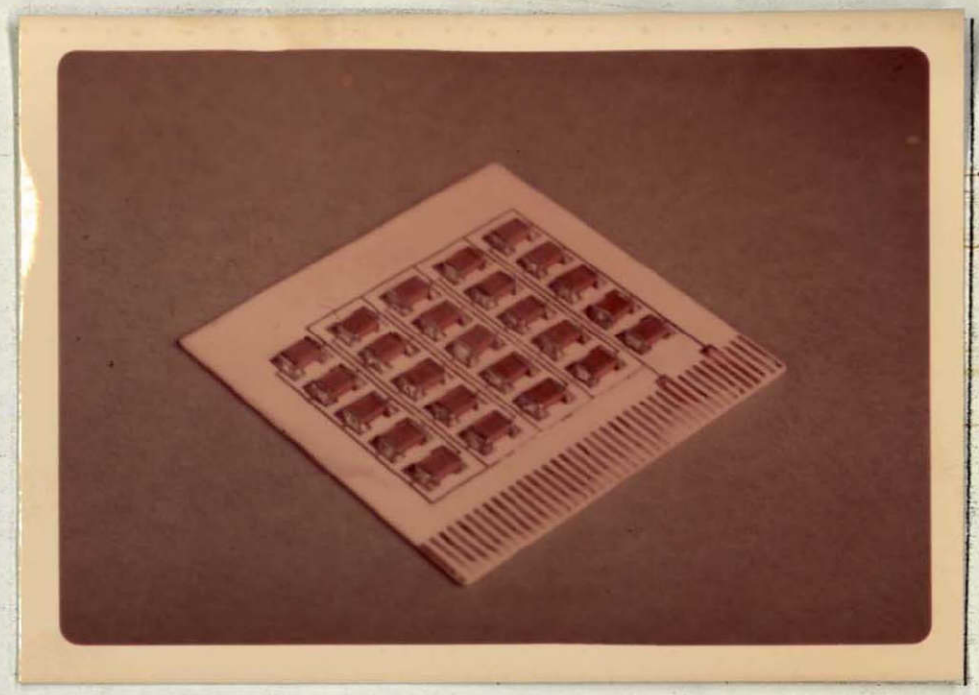

Figure 8C. Photograph of the thermal cycling test substrates as prepared 97.5 Pb 1.5 Ag 1 Sn.

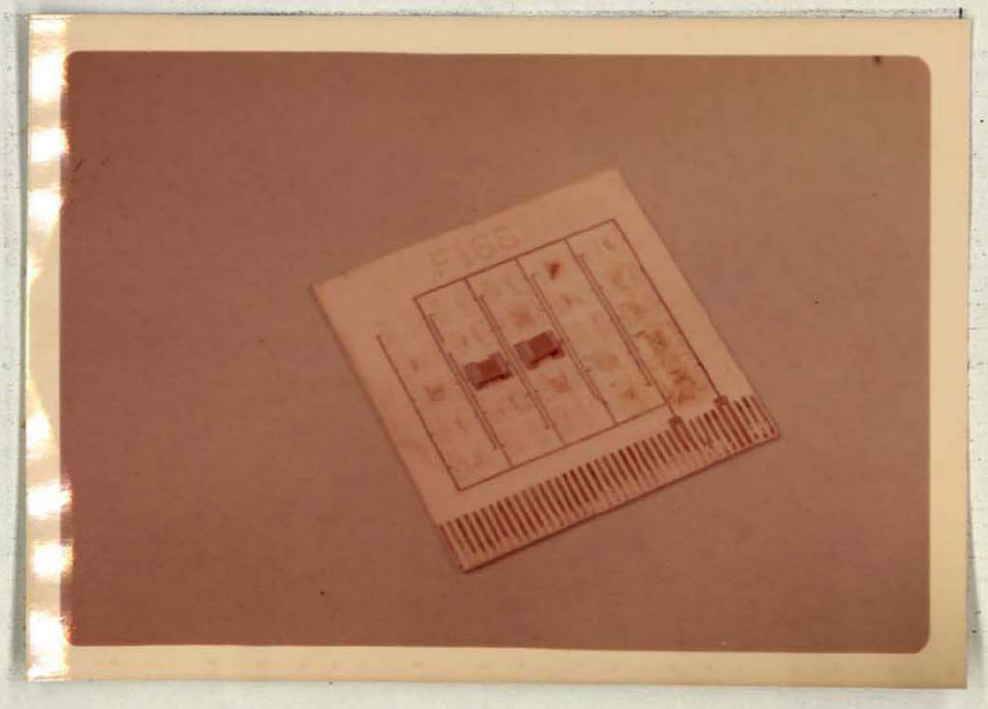

Figure 8D. Photograph of the thermal cycling test substrates 97.5 Pb 1.5 Ag 1 Sn after 1000 cycles.

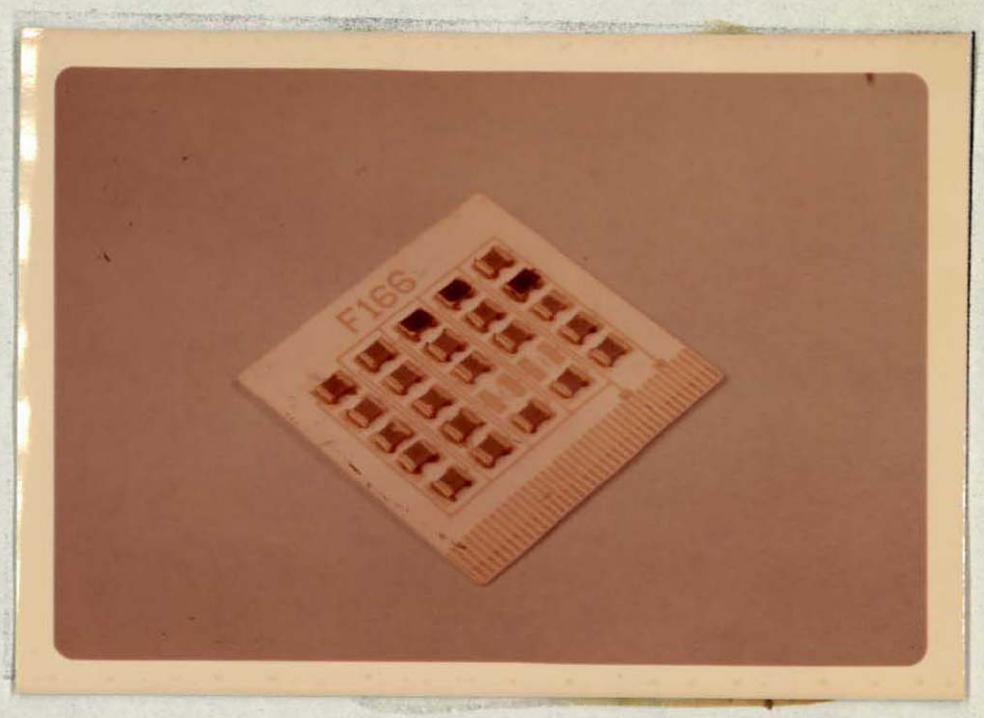

Figure 8E. Photograph of the thermal cycling test substrates gold filled epoxy after 1000 cycles.

the as prepared test system. Figure 8D is the same substrate after 1000 thermal cycles and most notable exhibits missing metallization as well as the characteristic loss of solder luster mentioned above. The metallization degradation in this system is just short of total destruction and points to a new problem of metallization stability during thermal cycling. Figure 8E is of the gold-filled epoxy system after 1000 cycles in which the system failure rate is only 10% (Two capacitor chips were defective before thermal cycling and were removed, hence, more failures are present than were caused by thermal cycling.)

The pictures presented above, the failure rate observations and the destructive physical analysis of the solders indicate that they do not meet high reliability standards. The one gold-filled epoxy system examined exhibits significantly higher reliability than any of the soldered systems but failure rates are still of great concern in the epoxy system.

Thick Film Resistor Material Studies

The thick film resistor studies have focused primarily upon resistor compositions of the iron oxide-phosphate and vanadium oxide-phosphate systems with appropriate metallic additions. The iron results were summarized in a preliminary state of completion and analysis in last year's final report. The completed data and analysis in this series of resistor compositions is presented in the attached M.S. thesis entitled "Iron Phosphate Glass as a Thick Film Resistor Paste" prepared by Mr. S. M. Graff, the student supported under this contract.

The vanadium-phosphate resistor studies presently in progress have consisted of the preparation of thick film printable pastes from premelted and ground 70 V_2O_5 30 P_2O_5 glasses. These materials have been mixed with an organic vehicle and bonding agent in a manner similar to that employed for the iron work described

in the attached thesis. The printed paste was dried and then fired in a conventional thick film belt furnace under atmospheres of air, nitrogen and hydrogen. The peak firing temperature was examined over the range from 350°C to 650°C with markedly variable results.

The resistors fired on the lower end of the temperature, 350°C - 400°C, range resulted in granular crystalline appearing products with very poor adherence to the substrate. As the temperature was increased to the 500°C range, an excellent product was produced with a high quality bond and a ceramic black appearance. At higher temperatures, the product had a vitreous black appearance but the unprinted substrate adjacent to the resistor was discolored by what appears to be a vapor transported oxide of vanadium. This product has the appearance of a bleeding out or ghosting on the substrate although the mass of the resistor has not wet or spread appreciably.

Vanadium Electrical Results

The vanadium pastes prepared as described above were examined to determine the specific resistivity, temperature coefficient of resistance and the voltage coefficient of resistance. The absolute value of the resistivity observed varied from around 20 Kohm/square for the air fired product to 125 Kohm/square for firing in nitrogen to greater than 1 Gohm/square for the hydrogen firing. The range of resistivities is thus well within the range which can be expected to be of value in applications.

The temperature coefficient of resistivity for the air and nitrogen products is shown in Figure 9. This plot indicates that the change in resistance at 125°C is around 100% increase and the change at -55°C is approaching 400% for the air fired product. The nitrogen fired resistor gives a much higher TCR and the resistance change at -55°C is approximately 1,000% decrease. This range of TCR

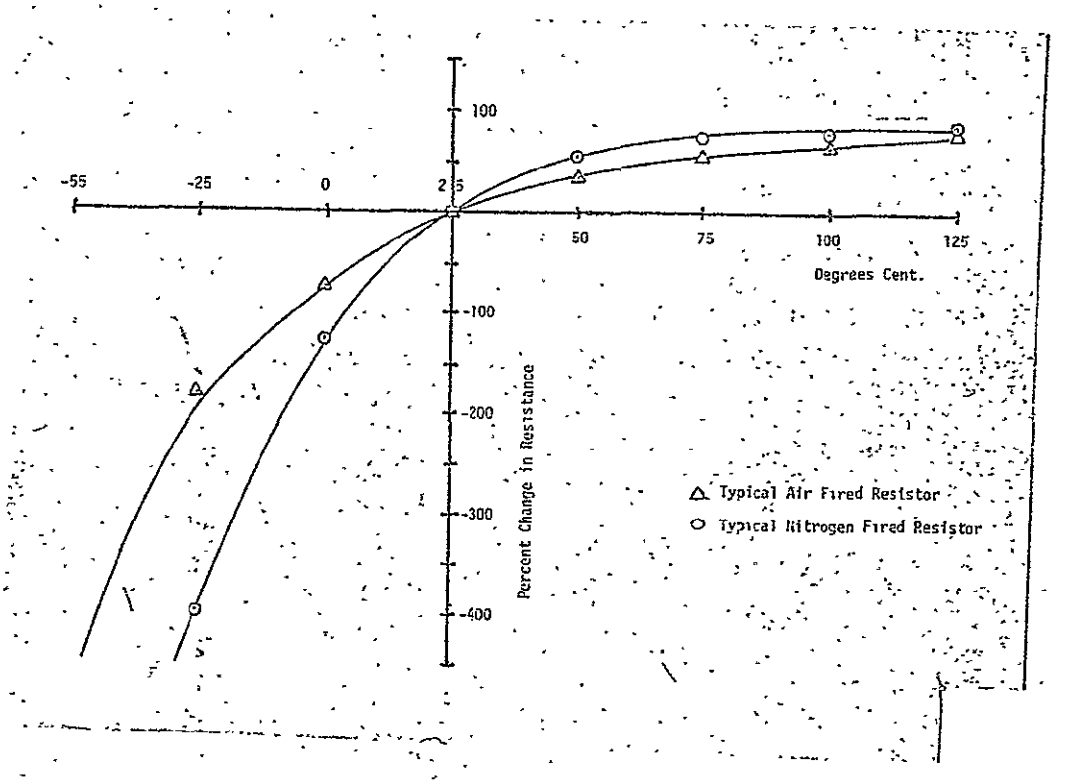

Figure 9. Resistance change as a function of temperature for the 70 V_2O_5-30 P_2O_5 paste fired as noted.

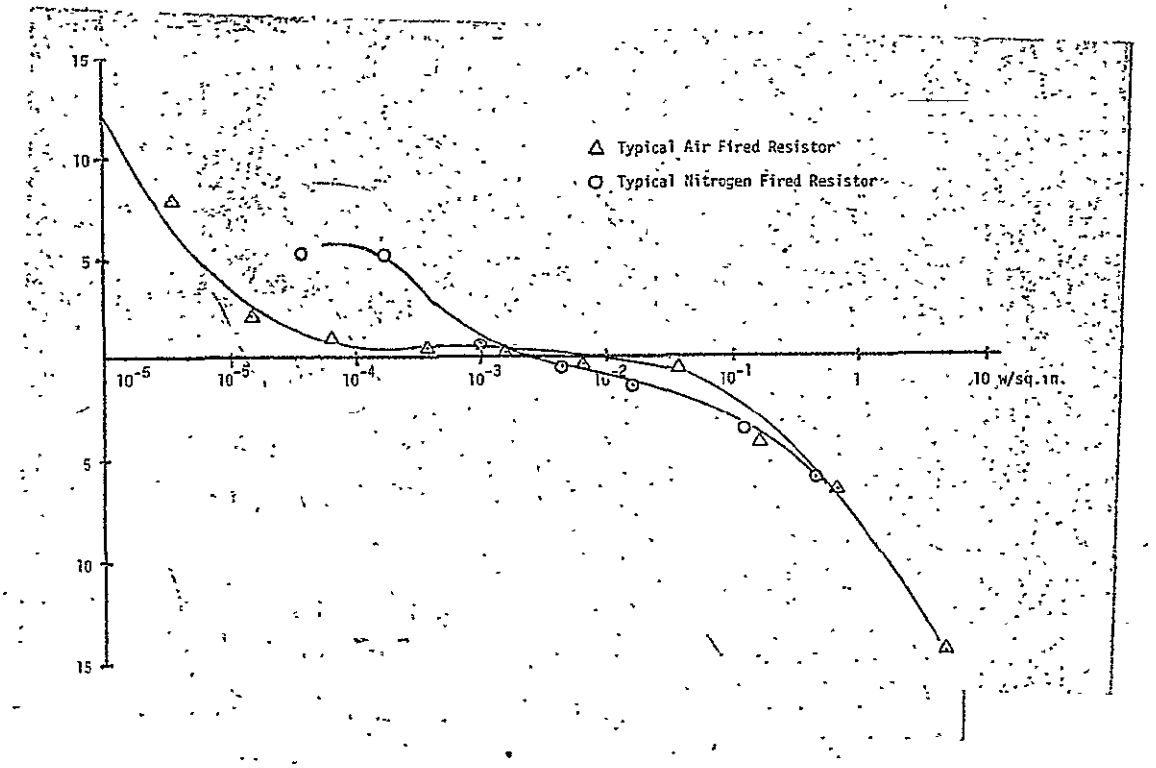

Figure 10. Resistance change as a function of specific power for the 70 V_2O_5-30 P_2O_5 resistors fired as noted.

values is probably far too high to be of significant value in circuit applications but may be of substantial application potential in thermistor applications. It is quite clear than an appropriate air/nitrogen mixture during firing can be employed to produce a wide range of TCR values as would be useful in thermistor applications.

The voltage sensitivity of the resistance is indicated in the plot of Figure 10 where the resistance change from 25°C is plotted as a function of power dissipation. For power dissipation levels in the range of 10^{-4} to 1 watt/square inch* these resistors exhibit less than a 5% change in value, This behavior is quite acceptable for most applications that may be envisioned for the thick film resistor material or the thermistor application.

It should be noted that considerable attention is now focused upon high sensitivity thermistor materials for application in infrared sensing devices. These devices depend upon the focusing of IR energy on a low mass high thermal coefficient resistance element which then gives a resistance value proportional to the incident IR flux. The control of such devices has recently proven to be a major reliability problem in current sensing technology.

In summary, the present status of the thick film resistance program can be characterized as one of growing understanding. The iron data summarized in the attached thesis indicate substantial promise of application although some environmental stability problems are apparent.

The vanadium resistor materials appear to need considerable more work in order to explore the range of oxidation/reduction phenomena available to give lower TCR values. Some of the presently attained TCR ranges may find application in resistors designed to have high TCR values (i.e., thermistors).

---

*1 watt/square inch = .155 watt/cm^2.

Summary of Present Program

The present program has focused upon two phenomena: the bonding reliability of discrete components and the development of base metal thick film resistor materials. The bonding reliability has developed some firm conclusions regarding the advisibility of using the presently available solder and epoxy bonding systems as well as uncovering some new problems in thick film conductors. The conclusion is presently inescapable that solder bonded discrete components are not reliable enough for application in high quality hybrid microelectronic systems. The thick film degradation observed during thermal cycling is a newly reported phenomena which requires further analysis.

The thick film resistor studies have explored two different type transition metal oxide phosphate systems. The iron system has been developed to a tolerable although not high quality system from an electrical property point of view although it does suffer from environmental sensitivity. This sensitivity can be reduced as applications require by the addition of overcoating or compositional modification. The vanadium system has initially given resistors which have too high a TCR to justify the name resistor-thermistor is more appropriate. The thermistor application may in fact be an important application of these materials as present problems in IR sensors are potentially soluble with such materials.

Further Work

This program has reached some conclusions summarized above and the basic aspects of reliability of bonding during thermal cycling does not require additional work. The problem of metallization adhesion and degradation of metallization during thermal cycling raises a serious problem which should be examined in further work. The resistor paste materials studies have reached a preliminary state of development in which potential for both resistor and

thermistor development is demonstrated. This area requires further work in order to outline the processes and compositions which can be adapted to practical applications. It appears that oxidation/reduction treatments over a broader range of oxidation potential are likely to give products with substantially improved properties over the present results. It also appears that the oxidation potential during the firing operation gives an important tool for tailoring the particular paste to the intended application.

18

Reliability of Soldered Joints in Thermal Cycling Environments

Chip capacitors soldered to metalized alumina substrates exhibit high failure rates when subject to thermal cycling.

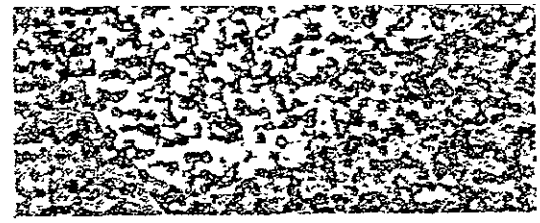

Microstructure of as-received 63/37 tin-lead solder (400x).

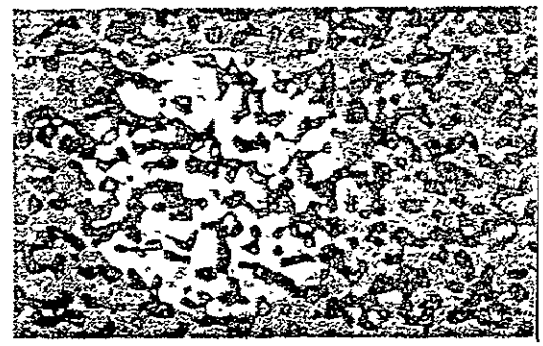

Microstructure of as-received 63/37 solder after 1,000 thermal cycles in free-standing position (400x).

By D. L. Kinser, J. G. Vaughan and S. M. Graff, Vanderbilt University, Department of Materials Science, Nashville, Tennessee

Failure of solder-bonded ceramic capacitor chips on alumina substrates has generally taken the form of chip rupture, termination failure, solder failure or substrate metallization failure. Previous experimental studies have addressed themselves to the calculation and measurement of the strain or stress induced into the capacitor chip during thermal cycling.[1,2]

The previous theoretical model of the capacitor chip/substrate system assumed that the substrate was rigid with respect to the chip and the bond was ideal, i.e., no shear was allowed in the bond. This model can be shown[1,2] to give a stress in the chip (σ) given by the equation:

$$\sigma = E_{chip} (\alpha_{chip} - \alpha_{sub})\Delta T$$

where E_{chip} is the Young's modulus of the chip, α_{chip} and α_{sub} are the thermal expansion coefficients of the chip and substrate respectively, and ΔT is the temperature change. This equation was used to calculate the change in stress from 25°C to −65°C and tensile stresses as large as 50,000 psi were computed. These results were based upon actual measurements of both thermal expansion and Young's modulus for the chips.

In the light of these extraordinarily high stresses it was apparent that most solder joints could be expected to shear or the capacitor body rupture. In an effort to examine the shear in the joints, an experimental measurement of the stress in the chips was then undertaken. This measurement consisted of placing a strain gage on the body of the capacitor chip and subjecting the system to a thermal excursion. With appropriate instrumental corrections this approach revealed that the actual stresses were of the order of 2,500 to 3,000 psi in the soldered systems. It was thus quite apparent that the soldered joints were yielding to the high stresses, and close examination indicates that the shear direction of deformation of the joint changed directions during the 25°C to +125°C to 25°C to −65°C cycle. This alternating load on the capacitor bond appeared to be the cause of the high failure rates of this type bonding system during thermal cycling.

This article involves the study of the joint failure rate as a function of soldering variables using metallurgical analysis of the joints. It was also necessary to thermally cycle a group of freestanding solder samples to examine the influence of thermal cycling in the absence of stresses from the solder joint.

Experimental technique

For purposes of experimental evaluation of processing variables, the substrate chosen was 96% alumina with a 25 μin. surface finish. The conductor metallization chosen was a standard solderable, high-reliability, platinum-gold, thick-film metallization. The solders chosen were eutectic type 63/37 tin-lead and 96/4 tin-silver. The ceramic capacitor chips employed in this study were 10^4 picofarad ±20%, 50-V rated, with BX-type dielectric. The capacitor terminations were pretinned by the vendor with solder of the above mentioned types. The physical dimensions of these capacitors were 0.175 x 0.125 x 0.060 in.

The capacitors were mounted on a standard metallization pattern with 25 chips on each substrate. The metallization was printed, dried and fired in accord with the manufacturers instructions. The substrates were pretinned after fluxing by dipping for 5 s at 300°C for 63/37 solder and 250°C for 96/4 solder. The substrate were removed from the tinning bath in a vertical position to facilitate drainage of excess solder. The capacitors were placed in their positions, and the substrate was placed on a hotplate at 300°C for 63/37 solder and 250°C for 96/4 solder, where it was held until the solder flowed or for approximately 5 s and then cooled as shown in Fig. 1. The two basic cooling rates were obtained by placing the substrate on a room temperature aluminum block and by cooling on the hotplate with insulation to allow slow cooling.

After the soldering operation, the flux was removed from the substrates with toluene and the solder joints were visually inspected. One group of bonded capacitors was subsequently

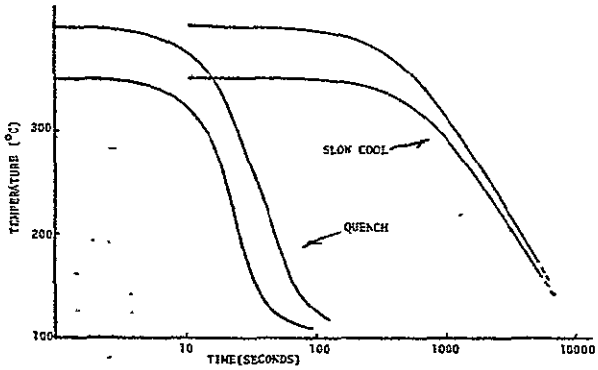

1. Cooling curves for the soldering process. Quenching corresponds to removing the substrate from heat source and placing on cold aluminum block. Slow cool corresponds to cooling the sample on a hot plate with insulation.

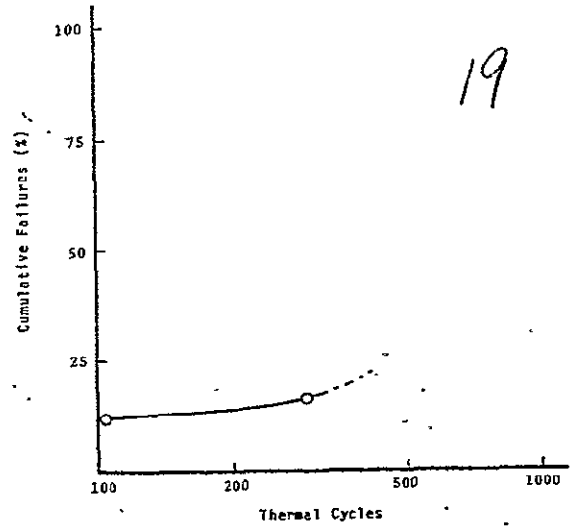

2. Cumulative failures as a function of number of thermal cycles for samples of 63/37 tin-lead without a pretinning treatment.

subjected to ultrasonic stress-relief treatment. This operation was conducted in a conventional cleaning type ultrasonic unit by immersing the substrate in benzene and operating the unit for 120 min. After the substrates had been prepared as described above, they were thermally cycled using a specially designed apparatus. This apparatus consisted of an insulated chamber held at +125°C + 2°C, a second chamber cooled by dry ice at −55°C, and a mechanical arm to transfer the samples from ambient to each chamber. This allowed the standard cycle of 15 min at ambient, 15 min at +125°C, 15 min at ambient and 15 min at −55°C to be repeated for up to 1,000 cycles. The initial setup employed an electrical monitor of each substrate which detected the electrical failure of a single chip on any of the 10 substrates in the test apparatus. This monitor was changed to a manual monitor in the cycling because of electrical connection problems to the substrate caused by alternate icing and melting. The final results are thus the collective data from electrical monitoring and visual inspections conducted after each 10 to 40 cycles.

In the course of thermal cycling, samples were removed at several times and destructively analyzed using metallographic techniques. The ceramic chip, solder, metallization and substrate were sectioned using a diamond saw, and the cross section of the solder joint was prepared using special metallographic techniques. A group of free-standing samples were also subjected to the thermal cycling and these were examined at various times throughout the thermal cycling to note any changes in the unstrained solder.

Results

The results of these experiments are presented in the form of cumulative percentage of failures as a function of number of thermal cycles. The results of cycling on the 63/37 soldered system without pretinning of the substrate metallization are shown in Fig. 2. The data here are quite scanty because the high failure rate at 100 cycles caused termination of the cycling at 300 cycles where the failure rate reached 18%. It is apparent that the reliability of capacitors bonded with this technique is most unsatisfactory for use in high-reliability systems.

The results of the customary soldering operation with 63/37 solder with a rapid quench from the soldering temperature are shown in Fig. 3. The failure rate in this system reaches 20% at 600 cycles and is thus considerably

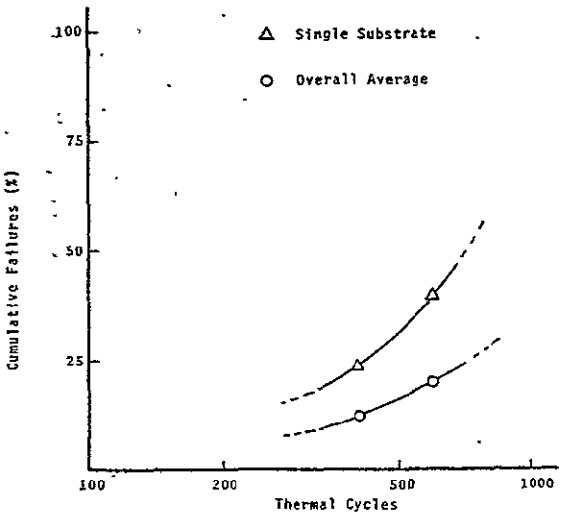

3. Cumulative failures as a function of number of thermal cycles for samples of 63/37 quenched from the soldering temperature.

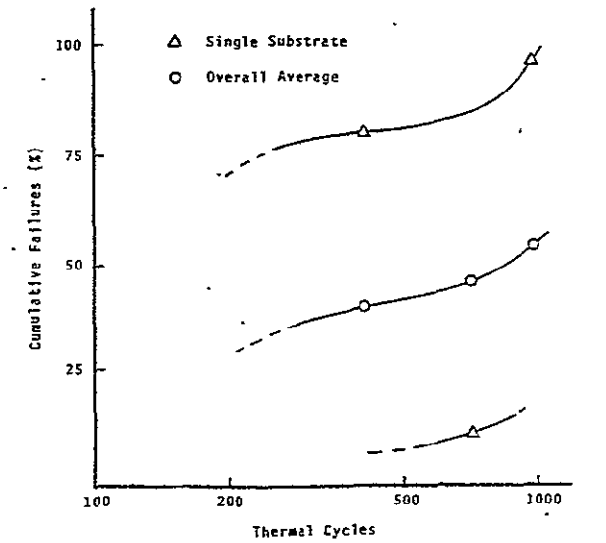

4. Cumulative failures as a number of thermal cycles for samples of 63/37 slow cooled from the soldering temperature.

better than the untinned technique, but the system is certainly unacceptable at this high number of cycles. It should be noted that reproducibility of this soldering technique was quite variable. Two substrates with a total of 100 bonds (50 chips) were cycled and one of the substrates with 50 bonds survived the 1,000 cycles with no failures. The data, however, are based upon two substrates and the poorer substrate suffered a 40% failure rate at 600 cycles; hence, the soldering technique is of questionable reproducibility. There are no known differences in the processing techniques for these substrates and it appears that the technique produces bonds of widely variable behavior. The results obtained on a 63/37 solder slowly cooled from the soldering temperature are shown in Fig. 4. It is apparent that the variation from substrate to substrate is large and high failure rates are noted. One of the substrates had 24 of the 25 capacitors with electrical failure (96% failure rate) at 1,000 cycles. The second substrate had only 16% failures at 700 cycles. Again, no processing variables were known to have changed during the process; hence, no explanation for the variability can be advanced. This substrate also exhibited a second failure mechanism not previously noted. The pretinned metallization lines on these substrates are severely degraded during thermal cycling and some electrical failures occurred in the metallization. This type behavior is apparent in the photograph shown in Fig. 5.

The results of cycling upon an ultrasonically stress-relief treatment has not enhanced the performance of

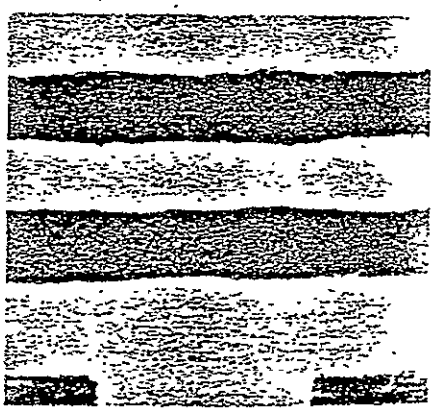

5. Typical metalization failure during thermal cycling. Illumination is from back of substrate to highlight the crack, thus metalization appears black.

this solder bond under thermal cycling (Fig 6). The best of the two substrates subjected to this treatment exhibited a 77% failure rate at 1,000 cycles, while the worst failure rate reached 96% at 900 cycles. The stress relief treatment has clearly degraded the performance of this solder, and the untreated system (Fig. 3 and 4) has clearly superior reliability.

The 96/4 Sn-Ag solder with a slow cool from soldering temperature was subjected to thermal cycling and the results are shown in Fig. 7. The variability from sample to sample in this system is considerably lower than in the 63/37 solders, but the overall reliability is unquestionably lower. This system exhibits failure rates as high as 38% at 265 cycles and is thus poorer than the Sn-Pb solder. The results of a 96/4 Sn-Ag solder quenched from soldering temperature to ambient are shown in Fig. 8. It is apparent that the variability from sample to sample in this system is small in comparison with all other samples examined. Unfortunately, the reliability of this solder is so low that 100% failure was reached at 850 cycles. Each class of capacitor solder bond was examined in a destructive manner by standard metallographic techniques. The capacitor-bond-substrate was sectioned along the longitudinal axis of the capacitor perpendicular to the substrate using a diamond saw, and the resulting section was metallographically polished using diamond abrasives. A typical example of the microstructure of the 63/37 solder joint before thermal cycling is shown in Fig. 9. This micrograph shows primary tin, idiomorphic particles, in a eutectic matrix of lead and tin. The structure of this same type joint after 1,000 thermal cycles is shown in Fig. 10. The primary particles have completely disappeared and only the eutectic tin-lead matrix is left. The microstructure of the thermally cycled joint is thus clearly finer than the initial joint structure.

The results of studies of the unconstrained solder are shown on the title-page for the as-received and 1,000 thermal cycles sample, respectively. The as-received microstructure is fine and the cycled sample is clearly coarsened by thermal cycling.

The ultrasonic stress relief treatments upon the solder joint should have decreased the residual stress and thus increase the reliability of the system. The observed effect of this treatment is to render this particular system and treatment the least reliable of the family of 63/37 solder treatments examined. This may possibly be the result of too long stress relief, resulting in the initiation of cracks by mechanical fatigue in the solder, but detailed scanning electron microscopy will be necessary to confirm this failure mode.

In the course of this study we have also noted a previously unreported failure mode in the substrate metallization. This failure mode takes the form of a reaction between the solder and the platinum/gold metallization and leads to loss of electrical continuity in the conductor. This may be the consequence of two possible failure modes. The most likely mode appears to be the differential thermal expansion between substrate, substrate metallization, and solder. None of these components can be expected to have the same thermal expansion coefficient; hence, mechanical stresses are created during thermal cycling. This could lead to the observed cracking and is supported by the preponderance of cracks initiating at the corners and other locations of stress concentration. The second possible metallization/solder failure mode is the formation of an intermetallic compound or compounds by interdiffusion of the solder and substrate metallization. There are four elements present to form intermetallic compounds hence there are almost innumerable possible intermetallic compounds which can be formed.

A separate observation made in the course of this study was the severe degradation of the metallization which had been pretinned. Many of the conductors were severely eroded from points near corners and other stress concentrators, and some of the conductors had actual cracks which resulted in electrical opens. Figure 5 is an example of the more severe state of this phenomena and shows the complete breakage of the metallization utilizing backlighting of the substrate.

Discussion of results

The results of soldering process variables upon the failure behavior during thermal cycling are summarized in Fig. 11. It is apparent that the most reliable system examined is the 63/37 solder quenched from the soldering temperature. The next most reliable bonding system is the untinned 63/37 quenched from the soldering temperature. The remaining soldering systems are clearly distinguished from one another but the reliability of all

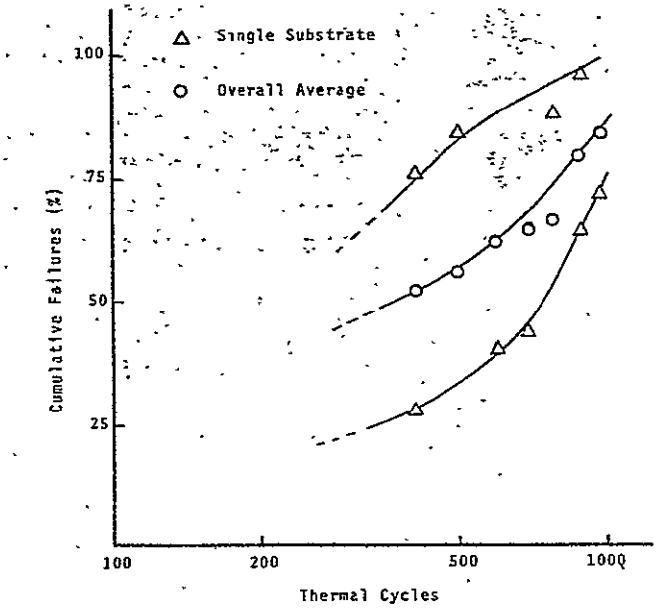

6. Cumulative failures as a function of number of thermal cycles for samples of 63/37 slow cooled and ultrasonically stress relieved before thermal cycling.

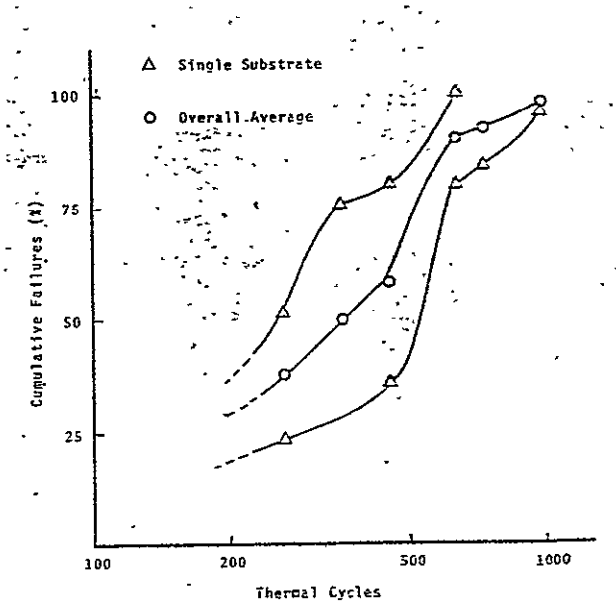

7 Cumulative failures as a function of number of thermal cycles for samples of 96/4 tin-silver slow cooled from the soldering temperature.

these systems leaves much to be desired. The microstructural studies of the free standing solder and of solder constrained by the joint indicated that the unrestrained solder structure coarsened while that in a joint was refined. This is a clear indication that the solder is being subjected to mechanical strain during the thermal cycling. The influence of the finer structure upon the mechanical strength of the joint is to give it more strength. This leads to the apparent anomaly of a stronger joint developing during thermal cycling, but still failing. This is the consequence of our original theoretical predictions. If the joint is ideally rigid (in this case only more nearly rigid), then the stresses in the bond rise to values which must lead to failure. In fact, the evidence indicates that the joint indeed becomes stronger during thermal cycling, and this is the cause of thermal cycling failure. The solder which is not constrained in a joint simply coarsens and, as a consequence, becomes weaker.

In conclusion, solder bonded systems which have been examined in this program are far too unreliable to be seriously considered for use in high-reliability space military systems. The cause of failure appears to be a strengthening of the solder by repeated strain during thermal cycling. This stronger solder does not deform as a virgin joint, hence, the thermal expansion mismatch stress climb to levels at which joint failure occurs.

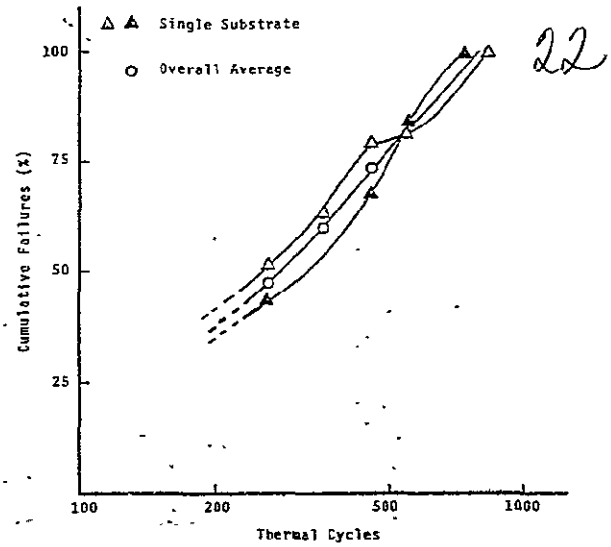

8. Cumulative failures as a function of number of thermal cycles for samples of 96/4 quenched from the soldering temperature.

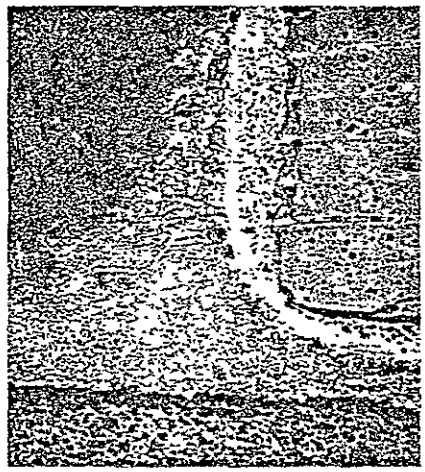

9. Typical microstructure of 63/37 solder joint (160x).

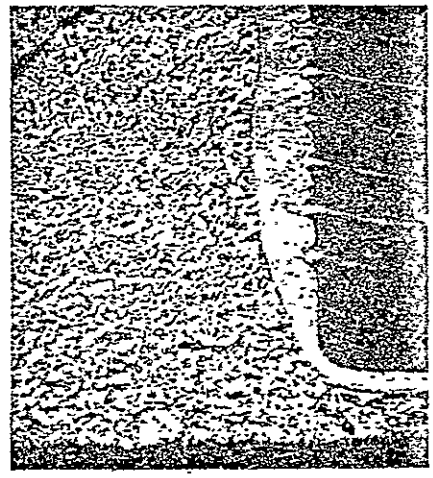

10. Typical microstructure of 63/37 solder joint after 1,000 thermal cycles (160x).

Acknowledgments

The authors wish to gratefully acknowledge the encouragement and technical discussions with Mr. S. V. Caruso of Marshall Space Flight Center and the financial support of the National Aeronautics and Space Administration under Contracts NAS 8-30883 and NAS 8-29460.

References

1. D. L Kinser, S. M. Graff and S. V Caruso, "The Relationship Between Reliability and Bonding Techniques in Hybrid Systems," *IEEE Trans on Parts, Hybrids and Packaging, PHP 11* (3) September, 1975.
2. S. S. Cole and A. R. Kroehs, "Stress Failures and Joining Considerations in Hybrid Circuits," *Proceedings Electronic Components Conference*, April, 1969.

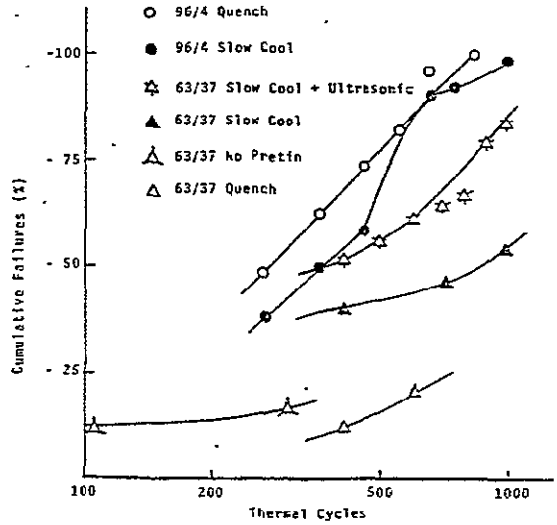

11. Summary of the overall cumulative failure behaviour as a function of number of thermal cycles.

IRON PHOSPHATE GLASS AS A THICK FILM RESISTOR PASTE

By

Stephen M. Graff

Thesis

Submitted to the Faculty of the

Graduate School of Vanderbilt University

in partial fulfillment of the requirements

for the degree of

MASTER OF SCIENCE

in

Electrical Engineering

December, 1975

Nashville, Tennessee

Approved: Date:

_____ _____

_____ _____

_____ _____

IRON PHOSPHATE GLASS AS A THICK FILM RESISTOR PASTE

STEPHEN M. GRAFF

Thesis under the direction of Professor Donald L. Kinser

Recent studies of electrical conductivity in transition metal oxide glasses suggested a possible alternative to the noble metal pastes used in thick film circuits. As an initial candidate, iron phosphate glass was ground and combined with an organic vehicle of alpha terpineol and ethyl cellulose to form a thick film resistor paste. Glass frits of different average particle sizes were combined in varying amounts of the organic vehicle to attain optimum printability. Alpha terpineol was the vehicle for printing and ethyl cellulose was the binder during the drying process. Viscosity was controlled by the relative amounts of alpha terpineol and glass frit. Thinners, used as needed after storage, were diethylene glycol monobutyl ether and diethylene glycol monoethyl ether. Resistors of one square, multi-square and sub-square geometries were utilized in the test pattern including large probe pads for resistance measurements. Compatible conductor pastes were selected from the commercially available pastes.

Resistivity was studied as a function of composition, firing temperatures, firing rates, and voltage and temperature coefficients of resistance (VCR and TCR). Conductance in iron phosphate glass depends on the relative concentrations of the two valence states of iron and the relative amounts of iron and phosphate. Firing rates and temperatures were adjusted to allow for proper expulsion of the organic vehicle and binder. Microstructure and bonding of the resistor material were affected by the sintering process. VCR and TCR were affected by the printing and firing process and the composition of the resistance material. Electrical and environmental tests were used to optimize processing and material selection.

Approved_____ Date_____
Adviser

DEDICATION

I wish to dedicate this thesis to my wife Michele who endured patiently and encouraged the completion of this research.

ACKNOWLEDGMENTS

The author wishes to sincerely thank his advisor, Dr. D. L. Kinser, for his help and guidance during the course of this research. He would also like to thank Mr. J. G. Vaughan for his helpful discussions and gratefully acknowledge Mr. J. Hightower and Mr. R. McReynolds for their assistance in setting up and maintaining the equipment.

This research was undertaken through the National Aeronautics and Space Administration/Marshall Space Flight Center, Contract No. NAS8-30883.

17

TABLE OF CONTENTS

		Page
LIST OF TABLES		v
LIST OF FIGURES		vi
Chapter		
I.	INTRODUCTION	1
II.	THEORY AND LITERATURE SEARCH	3
	Artwork	3
	Rheology	4
	Firing Process	7
	Iron Phosphate Glass	7
III.	EXPERIMENTAL PROCEDURE	13
	Glass Melting	13
	Frit Preparation	17
	Organic Vehicle	17
	Paste Mixing	18
	Conductors	19
	Pattern Mask and Screen Preparation	19
	Printing Procedure and Equipment	20
	Firing Procedure and Equipment	20
	Electrical and Environmental	23
IV.	EXPERIMENTAL RESULTS	25
V.	DISCUSSION OF RESULTS	33
	Rheology	33
	Firing Characteristics	35
	Electrical Characteristics	36
VI.	CONCLUSIONS	41
	Notes on Future Research	42
LIST OF REFERENCES		44

28

LIST OF TABLES

Table		Page
1.	Atomic Percentage Breakdown of Iron Phosphate Glasses	14
2.	Paste Compositions Studied	15
3.	Relative Adhesion as Related to Firing Condition	27
4.	Resistance as Related to Reducing Atmosphere Firing	29
5.	336 Hour Room Storage Date	30

29

LIST OF FIGURES

Figure		Page
1.	Temperature as a Function of Time for the Programmable Furnace (Firing Profile)	8
2.	Variation of Sheet Resistance with Firing Temperature (Belt Speed: 2"/min. 40 V_2O_5 · 60 TeO_2)	10
3.	Variation of Sheet Resistance with Belt Speed (Peak Temperature: 530°C - 40 V_2O_5 · 60 TeO_2)	11
4.	Block Diagram of the Programmable Furnace	21
5.	Reducing Atmosphere Gradient Furnace	22
6.	VCR Test Schematic	24
7.	Backlighted Photograph of Thick Film Prints	26
8.	Resistance as a Function of Temperature for the Three Pastes Examined	31
9.	Resistance Change as a Function of Power Dissipation	32
10.	Log_{10} Resistivity vs. 1000/T for Specimens 102, 104, 162, and 403	37
11.	Logarithmic Variation in the Conductivity of FeO in Terms of the Temperature Reciprocal	39
12.	Voltage Versus Current Plot for Pastes A, B, and C	40

CHAPTER I

INTRODUCTION

The first thick film resistors were carbon compositions,[1] but resistance drift due to age, use and environment rendered these resistors unsuitable in many cases. Inorganic systems were developed because final resistance value was set in the sintering process and the ceramic systems added stability to the resistors.[2] The conduction mechanisms in present systems are not completely understood, although compositions of the resistor pastes control the basic resistor characteristics. Resistance value is processing dependent and each user screens and fires his own circuits. Vendor specifications are the results of sample screening and firing by the vendor and users must screen to the same thickness and fire with the same profile to attain similar results.

Transition metal oxide glasses have been considered as a resistance system and Robertson[3] in his report on pastes made from vanadium tellurite and vanadium phosphate glasses indicated that transition metal oxide glasses had great potential as thick film resistors. Vaughan and Kinser's[4] study of conductivity in iron phosphate glasses has suggested strong potential in those glasses as a thick film resistor.

Thick film resistor pastes were made from several iron phosphate glass compositions. The effect of firing cycle and composition are correlated with electrical measurements including resistance, voltage and temperature coefficients of resistance and room temperature storage.

CHAPTER II

THEORY AND LITERATURE SEARCH

General information about thick film hybrid microcircuit production concerning the areas of the field important to this research included artwork, rheology (screen printing), and the firing process. The first part of this section will be concerned with the general research on thick film circuit processes and the last part with previous research on iron phosphate glass and a background of transition metal oxides as thick film resistors.

Artwork

Artwork in hybrid microelectronics is used to produce the screens discussed in the next section. The layout or arrangement of discrete components and resistor, conductor, and dielectric patterns are usually drawn on a 10:1 scale. Scales of 20:1 are used for high resolution in fine line products and scales of 1:1 for low density products. Actual size patterns of the conductive, resistive, and dielectric lines are printed on a glass slide.

Computer aided design (CAD) techniques have been developed for layout problems.[5] Elements should be arranged so that conductors are short and crossovers are avoided. Maximum width lines and largest possible terminal pads near

the edges and minimum conductor line separation are some desirable characteristics of thick film circuits. Algorithms for computer programs have been developed for this purpose.

Layouts are produced as "tapeups."[6] Colored tape is used to represent the respective lines. The use of "back lighting" and filters allows photographic reproduction of separate glass slides for conductor, resistor and dielectric regions.

Layouts may also be digitized on an x-y coordinate system for the Mann-pattern generator.[7] The system uses a series of shutters and a laser which draws the patterns directly on a glass slide. National Aeronautics and Space Administration standard resistor pattern F100E was supplied for this research by NASA/MSFC in the glass slide form as produced by their Mann-pattern generator.

Rheology

Stainless steel mesh screens are used and may vary from 200 to 400 mesh. An emulsion which hardens when exposed to ultraviolet light is spread evenly over the screen. A glass slide of the desired pattern is placed over the screen which is exposed to the ultraviolet light. The emulsion hardens except under the pattern lines and the soft emulsion is rinsed away leaving the desired pattern.

Circuits are printed by layers usually starting with the conductive layers followed by the resistive layers.

The screen of the desired pattern and an appropriate substrate is selected. The screen is connnected to the screen printer above the substrate mount and the screen pattern positioned in the center of the substrate. Paste is forced through the screen pattern with a squeegee. Speed, angle and pressure of the squeegee blade determines snap-off,[8] the point at which the screen and substrate separate. If the snap-off is too slow, the pressure is too strong and the print will be too thick. If the squeegee pressure is too weak, the screen will not make good contact with the substrate and the print will be too light. Camber or bowing of the substrate effects squeegee pressure and thus snap-off is effected.

Printing machines with the ability to control the above variables are available,[9] and some printers have continuous squeegee pressure control to accommodate substrate camber. Speed and angle of the squeegee are adjustable and reproducible. Methods for evaluating squeegee pressure, angle, and snap-off were not available at the time of this work, but the squeegee speed was approximately measured with a stop watch and controlled with the pneumatic set screws to a speed of 6-8 inches per second.

Variables in the thick film pastes are another

quality control problem. The ideal ink is one that remains at rest on the substrate, but flows easily when passing through the screen.[10] Screenability of thick film pastes is a function of the surface energies of the screen, substrate, and the paste.[11] Screen and substrate surface energies below that of the paste permit better release of the screen and lower flow rates before and during print and drying operations. The paste used is made of the resistive material and an organic vehicle. The organic vehicle used in this research consists of two components: ethyl cellulose and alpha terpineol, where dry ethyl cellulose is dissolved in the liquid alpha terpineol. The liquid is the vehicle for the printing process and is dried out after the printing process is completed. Ethyl cellulose serves as a glue holding the resistive material on the substrate until it is burned off in the firing process. Viscosity of the paste was controlled by the relative amounts of resistive material, ethyl cellulose and alpha terpineol. Thixotropic properties are desirable in thick film resistor pastes. The paste should flow easily through the screen, but remain at rest once it has been deposited on the substrate. The viscosity should be low enough to allow some flow after printing to eliminate the rough surface inherent to the printing process, but flow should not occur to the degree that resistor dimension is changed. If drying should occur during

storage, the paste should be restored by adding thinners, not additional O.V. The ethyl cellulose will not vaporize at room temperature and the original amount is still present. Successive additions of O.V. containing ethyl cellulose will cause loss of viscosity control. Thinners recommended for the organic system should be used. The two thinners used with alpha terpineol were diethylene glycol monobutyl ether and diethylene glycol monoethyl ether.

Firing Process[12]

The firing process controls the resistance by effecting the time and rate of reactions during sintering. Profiles similar to those in industry were used in this work as shown in Figure 1. The preheat zone, approximately 300° - 350°C, for three minutes, burns off the organic binder. The hot zone sets the final characteristics of the resistor and the cooling zone stops the process. Commercial firing profiles may vary from 40 - 60 minutes with hot zones from 700° - 1000°C, eight to ten minutes long.

Iron Phosphate Glass

Many transition metal oxides form glasses with P_2O_5. Electrical properties, including semiconducting behavior exhibited by iron phosphate glass, have been studied by Vaughan[13] and Dozier.[14] Semiconducting behavior generally occurs when the transition metal exists in more than one

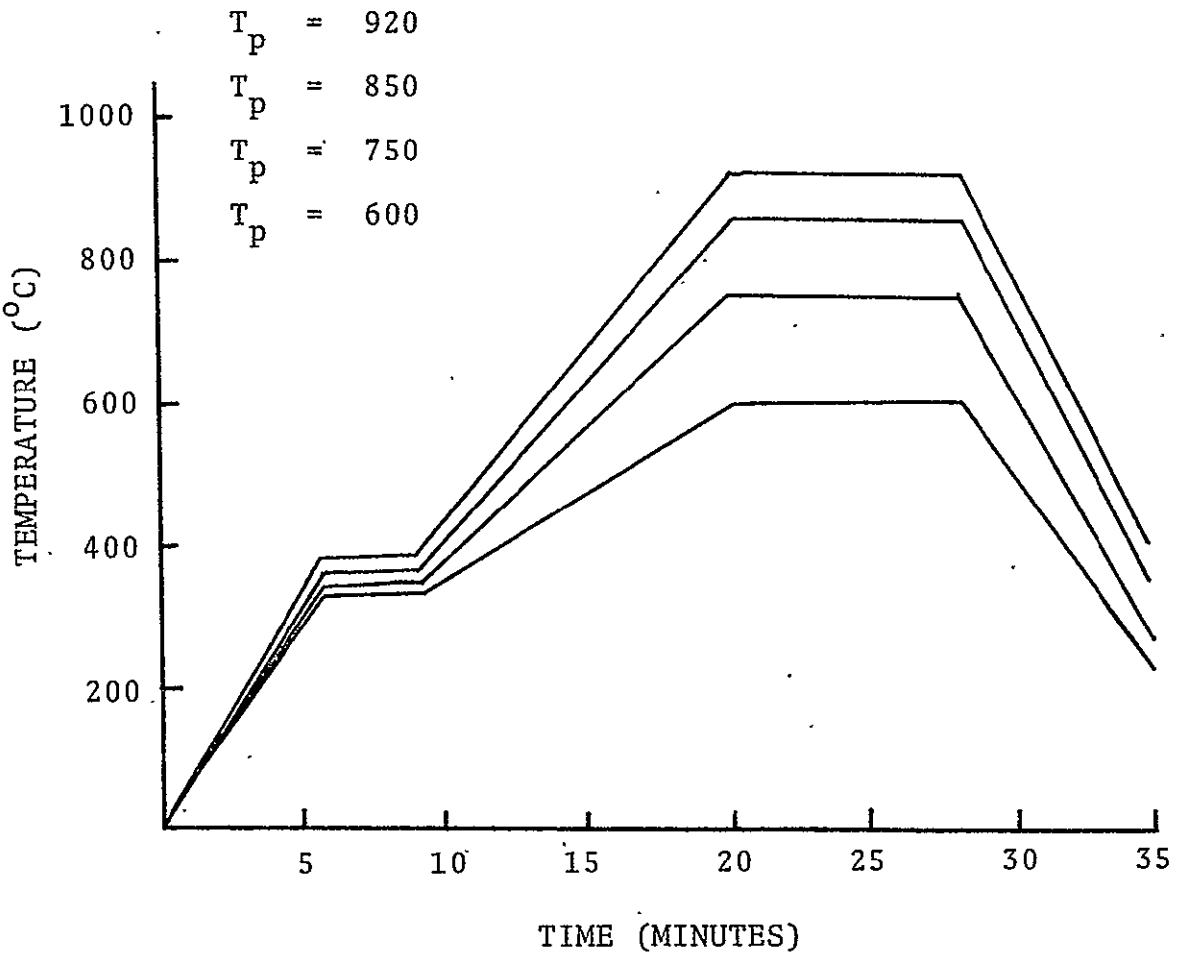

Figure 1. Temperature as a Function of Time for the Programmable Furnace (Firing Profile).

valence state. Conduction takes place by transfer of electrons from low valence to high valence states. Therefore the ratio of Fe^{2+}/Fe_{total} is important in controlling conductivity.

Robertson has performed similar research on two glass systems: $V_2O_5 \cdot P_2O_5$ and $V_2O_5 \cdot TeO_2$.[15] With the aid of a belt furnace, he showed the effects of oven profile on the final resistor. The belt speed was maintained at two inches per minute and the peak temperature was varied from 470° - 580°C. Figure 2 is a reprint of this data. Figure 3 is a reprint of the data for peak temperature held constant and belt speed varied from 2 - 6 inches per minute. These plots show that the resistance of the 40 $V_2O_5 \cdot 60$ TeO_2 glass was oven profile sensitive. Prints of the vanadium phosphate glass were less sensitive to changes in oven profile.[16] Resistance of the transition metal films can be controlled by controlling the valence states of the metal through firing in oxidizing, neutral, or reducing atmospheres. Robertson[17] fired one set of films under a neutral nitrogen atmosphere, but observed no significant differences in those films and air fired films. However, he noted that the furnace used was not designed for controlled atmosphere work and these results were not conclusive.

Electrical properties of vanadium phosphate pastes[18] fired in air were shown to be similar to the bulk glass

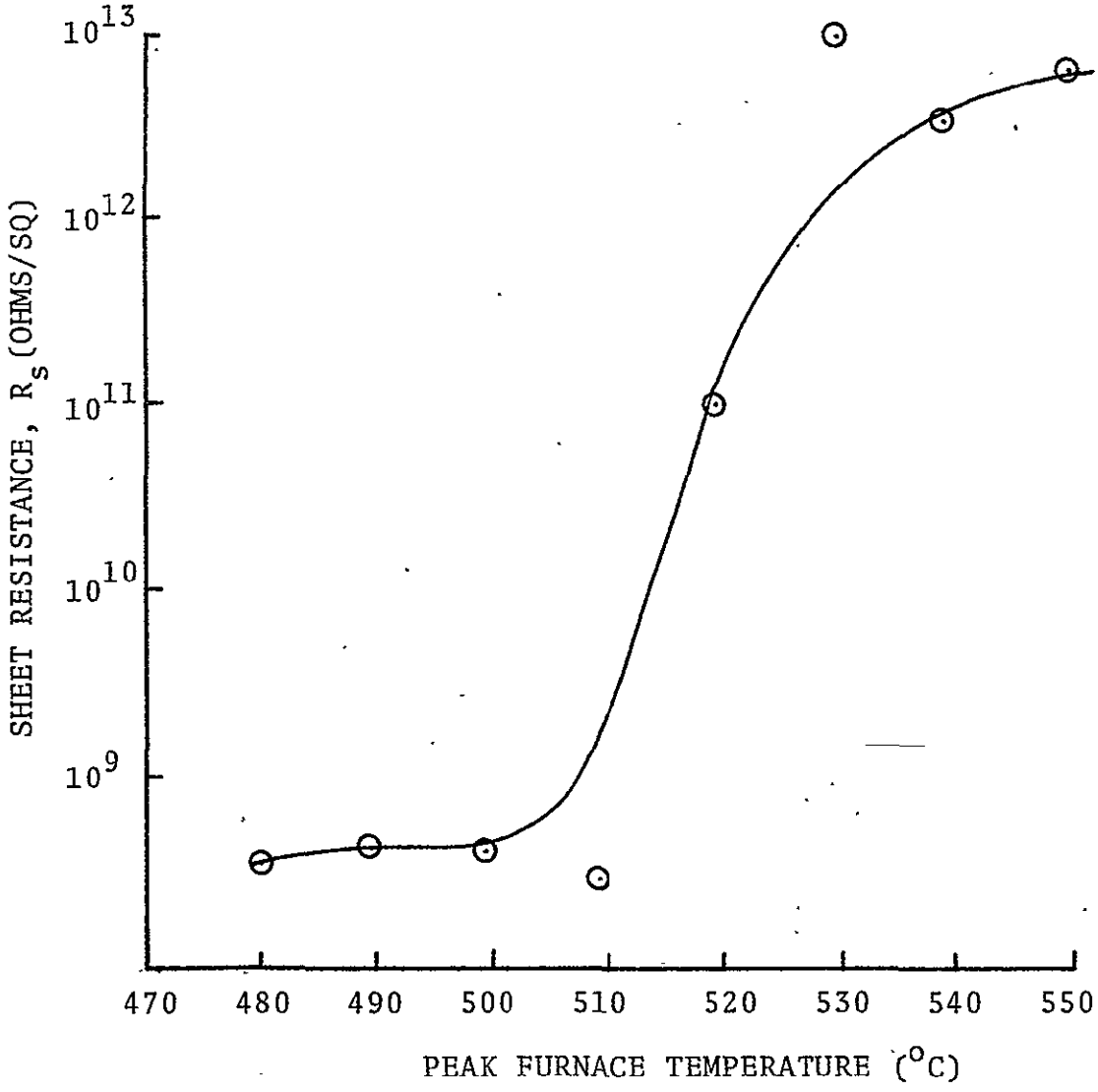

Figure 2. Variation of Sheet Resistance With Firing Temperature (Belt Speed: 2"/min-$40V_2O_5$-$60TeO_2$).[19]

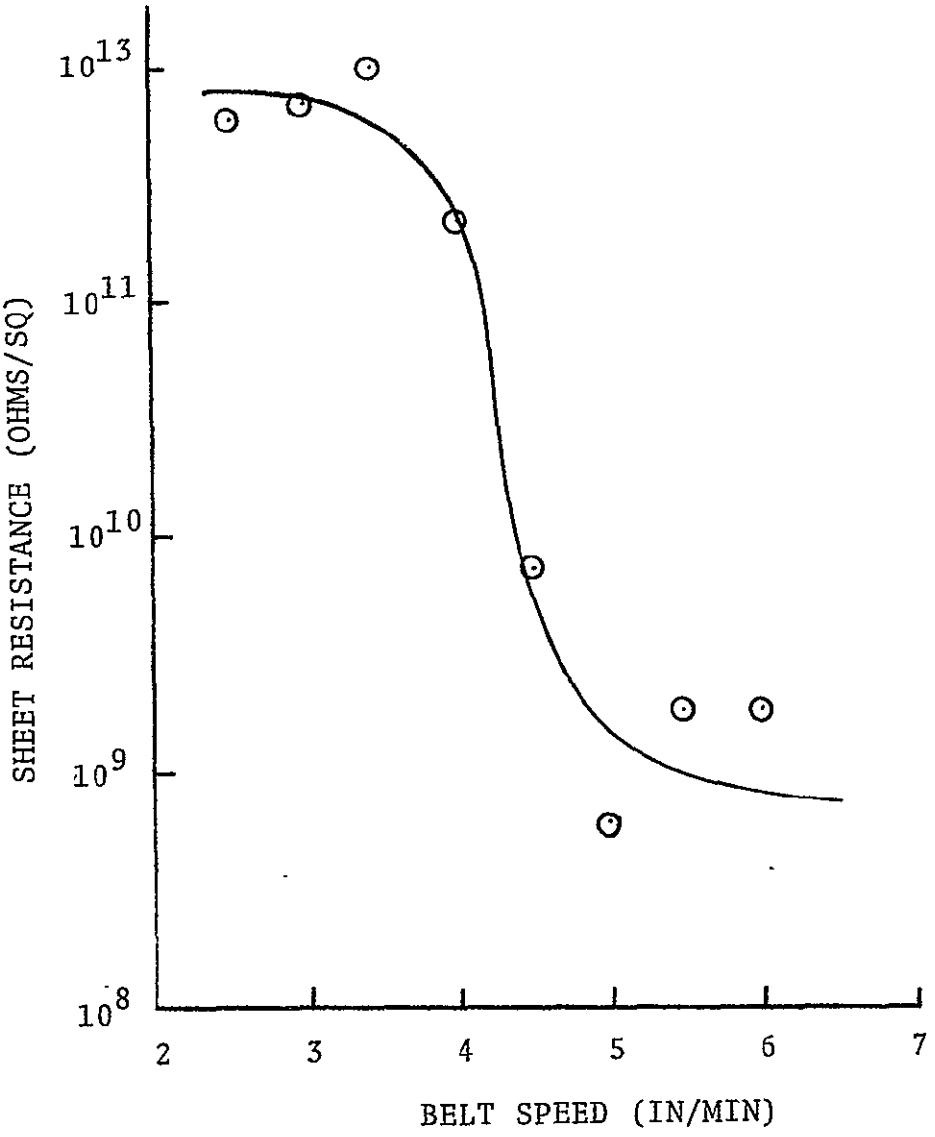

Figure 3. Variation of Sheet Resistance with Belt Speed (Peak Temperature: 530°C - $40V_2O_5$-$60TeO_2$).[20]

properties, however, the resistivities of some of the thick film pastes were two orders of magnitude greater than that of the bulk glass. Robertson[21] attributed probable cause to the differing thermal histories of the bulk glass.

Thermal histories of bulk glass samples have been shown to affect the conductivity of iron phosphate glass by Dozier et al.[22] Increasing quenching rates in the casting process decreases density and increases separation of the iron ions in the conduction system resulting in lower conductivity. Dozier[23] annealed bulk samples and altered the conductivity by changing the effective Fe^{2+}/Fe_{total} ratio. Preferential growth of crystals during annealing which effectively removes iron ions from the conduction system, also alters the resistivity of the bulk glass. The effects on conduction by magnetic coupling of the Fe^{2+} ions were noted by Friebele.[24] The magnetic coupling may tie up Fe^{2+} lowering the effective concentration of that ion. Removal of Fe^{3+} from the conduction process may occur if Fe^{3+} enters the glass as a former instead of a modifier.[25] Vaughan[26] found that bulk samples of iron phosphate glass behave as a glass having the combined effects of the magnetic coupling and microstructural influences stated above.

The pastes produced by Robertson acted as thermisters with temperature coefficients of resistance of approximately $3\%/^{o}K$.[27] Robertson indicated that the possiblity of better control may be attained by firing under a reducing atmosphere.

42

CHAPTER III

EXPERIMENTAL PROCEDURE

Glasses were chosen to give phosphate compositions from approximately 40 - 50% and Fe^{3+}/Fe_{total} ratios from 0.3 - 0.6 summarized in Table 1. Fe_2O_3 and iron powder were also added in some pastes to form compositions of 70 atomic percent total iron oxide and 70 atomic percent total iron. Test compositions are summarized in Table 2. The effect of composition on adherence and resistance was studied from these samples.

Glass Melting

The glasses used were available from the research of J. Vaughan of Vanderbilt University and this melting procedure is from his thesis.[28]

The glasses were made by melting batches in fused silica crucibles from thirty minutes to one hour at temperatures ranging from 1200°C to 1450°C. The batches were mixed from reagent grade materials (Fe_2O_3-P_2O_5) and were made in approximately 100 gram quantities. Individual components were weighed to within 0.1 gram, mixed in a container, and then shaken by hand for five minutes. The batch mixture was allowed to sit no longer than two hours before being added, a small amount at a time, to the crucible. The greatest

Table 1. Atomic Percentage Breakdown of Iron-Phosphate Glasses

Glass	FeO	Fe_2O_3	P_2O_5	Fe^{3+}/Fe^{tot}
123	30.5	24.1	45.4	0.612
142	42.0	8.33	49.7	0.284
163	23.0	17.0	60.0	0.596
422	33.2	7.7	59.1	0.317

Table 2. Paste Compositions Studied

	GLASS					
	FeO A/o	Fe_2O_3 A/o	P_2O_3 A/o	Added	Total Iron Oxide A.o	Total Iron A/o
A	23.0	17.0	60.0	--	40.0	--
B	33.2	7.7	59.1	Fe_2O_3	70.0	--
C	42.0	8.33	49.67	Fe	--	70.0

amounts of Fe_2O_3 versus FeO were obtained by melting in air for one hour at 1300°C. The ratio of FeO increased as dextrose was added in varying amounts to the melt; the carbon produced when the dextrose was burned reducing the Fe^{3+} ions. The greatest ratio of FeO was obtained by adding 100 grams of dextrose to the 100 gram batch and melting for only thirty minutes.

The specimens were made utilizing two 3 inch x 5 inch x 1/2 inch copper plates. A small amount of batch melt was poured on one plate and the other plate placed on top of the molten glass. The specimens obtained in this manner were normally 1/8 inch thick and approximately 1.5 inch in diameter. However, for the higher iron content glasses it was necessary to make glasses only 0.03 inches thick so as to obtain crystalline free specimens. It was found that the best specimens were obtained when the molds were kept at ambient temperature. After casting, the specimens were annealed at 300°C for one hour.

When the batch melts were poured, it was normally found that about five pours were necessary to empty the crucible. Thus, twenty to thirty minutes were usually required to pour all the batch specimens. Due to this time difference between pours, it was deemed necessary to use wet chemical techniques to determine if there existed compositional fluctuations among these different specimens. Of the five pours, titrations were run on the same group as the

electrical specimen and either one to two non-adjacent pours. The compositional variation between groups was found not to vary more than the error of titration; the error of titration being ± 1 percent by weight of iron.

Frit Preparation

Samples of iron phosphate glass of unknown composition were used to determine grinding and mixing procedures for paste fabrication. The glass was crushed to a particle size that would accomodate a Spex Mixer/Mill where the glass was ground to final size. The frit was sized in standard laboratory sieves to an average maximum dimension of 37 microns. After sieving, the frit was ground further in five minute intervals (5-10-15-20 minute frits). Samples of each frit were placed in the scanning electron microscope and sample averages were recorded. Industry standards indicate that the paste should be printable through a screen as small as 400 mesh, giving a maximum particle size of 38 microns (assuming 40% coverage by mesh wire). Preliminary work by printing several particle sizes indicated that an average particle size of 3 microns with an upper bound of 7 microns gave satisfactory print. Actual screens used in this research were 200 mesh (78.74 lines/cm).

Organic Vehicle

Two component organic vehicles were made by dissolving

dry ethyl cellulose in liquid alpha terpineol in ratios of 20.0 and 26.8 grams of ethyl cellulose per liter of alpha terpineol. The ethyl cellulose was weighed on a Mettler balance and the alpha terpineol was measured in a standard laboratory beaker. The ethyl cellulose was added to the liquid and slowly, magnetically stirred for approximately thirty minutes. Slow stirring was required to eliminate bubble formation in the final liquid, which effects the viscosity.

Paste Mixing

Organic vehicles of 20.0 and 26.8 grams per liter were mixed with samples of the glass frit to determine which organic vehicle made the most printable paste. The paste was mixed by hand after weighing the glass frit on the Mettler balance and slowly adding the O.V. from a pipet. Ratios of 2.2 to 3.8 grams of glass frit per milliliter of O.V. were used. Additional O.V. was not added after initial mixing. When drying occurred during storage, one or two drops of the available thinners were used to restore the paste to original consistency, thus the ethyl cellulose content was not affected. The thinners used were diethylene glycol monobutyl ether and diethylene glycol monoethyl ether. The liquid components of the O.V. used in the paste were the vehicle during the printing process and the ethyl cellulose was a glue during the firing process.

48

Conductors

Gold and platinum gold conductor pastes were chosen for the conductor lines. Gold was used for the in-air firing procedure, but the gold paste degraded severely under the hydrogen atmosphere. Platinum gold conductor was used in this application and the degradation was significantly reduced, but not eliminated. The degradation appeared to be a dewetting of the conductor line to the substrate, indicating a problem related to the glass frit binder. The components of the frit could have been reduced by the hydrogen atmosphere causing a loss of the glassy binder. The difference in the frit content of the two pastes used probably accounts for their differing reactions under the reducing atmosphere.

Pattern Mask and Screen Preparation

The glass slides used in the screen preparation were supplied by NASA/MSFC, S&E-ASTR-RMH Hybrid Microcircuit Section. A modification of NASA resistor test pattern F100E was used.

The screens were cleaned and soaked in stainless steel mesh prep, rinsed and dried. Sheet emulsion was cut and laid emulsion side up on a flat clean surface and the screen laid on the sheet. The liquid emulsion was sensitized and squeegeed onto the screen and the emulsion was dried for approximately thirty minutes. The plastic backing

was removed and the glass slide was positioned and taped into place. The emulsion was exposed for twenty-five minutes and rinsed with warm water leaving the pattern. The screen was dried and the parts of the pattern that were not used were painted out with stop-off lacquer.

Printing Procedure and Equipment

An AMI pneumatic screen printing system was used. Printing quality was controlled by squeegee speed and pressure and screen separation from the substrate. The squeegee speed was approximately adjusted to 6-8 inches per second. Methods for determining squeegee pressure and screen height were not available, but these controls were varied until an acceptable print was attained. Several substrates were printed for each paste. Conductor lines were dried and fired according to manufacturer specification.

Firing Procedure and Equipment

The substrates were marked according to the resistor paste used, peak firing temperature and the atmosphere of firing. The resistor paste was printed in the same manner as the conductor lines and was dried for thirty minutes at 80°C. The circuits were fired according to the profiles in Figure 1, in either air or hydrogen atmospheres. The programmable box furnace, shown in Figure 4, was used in air firing and Figure 5 shows the tube furnace used for the hydrogen atmosphere firing. The programmable furnace

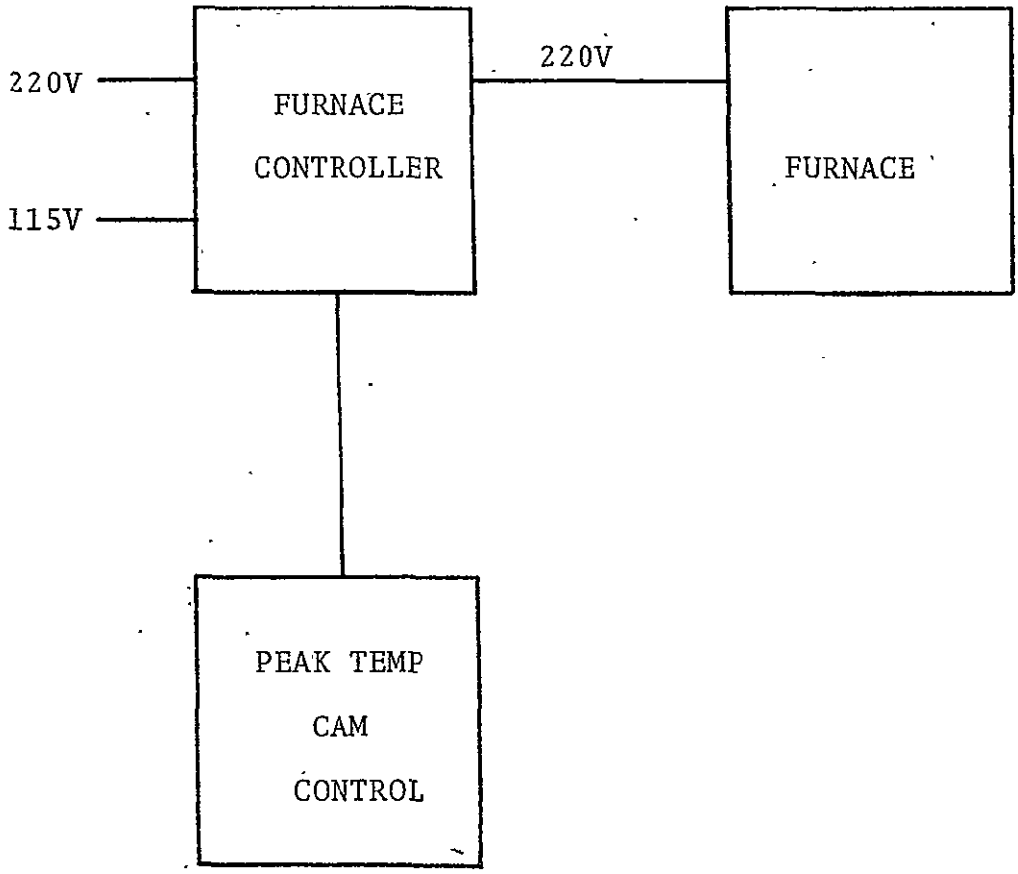

Figure 4. Block Diagram of the Programmable Furnace.

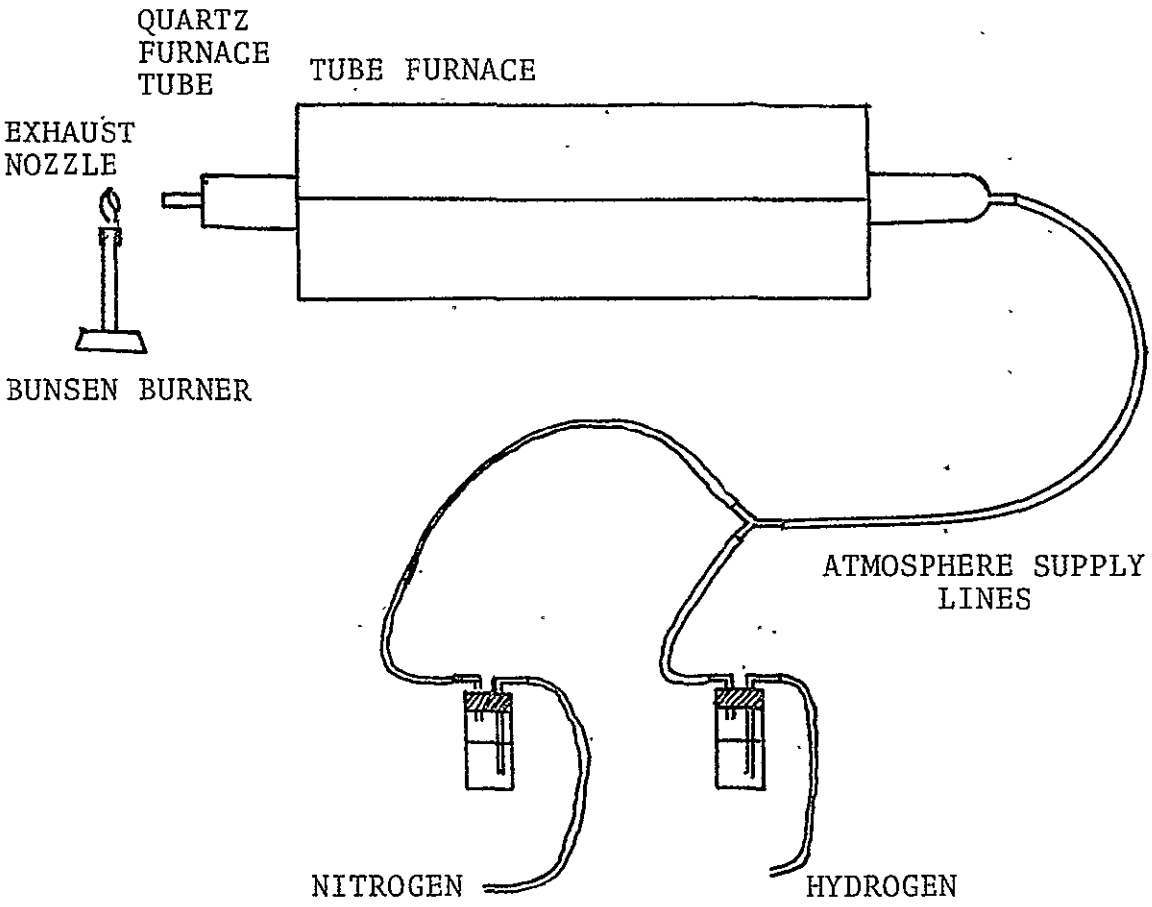

Figure 5. Reducing Atmosphere Gradient Furnace.

52

temperature was controlled according to time and the temperature of the tube furnace was controlled according to position in the tube.

Electrical and Environmental

Resistance was measured on two instruments, the Fluke Model No. 8000A/05 and the Digitec Model No. 245. The effect of temperature on resistance was evaluated from -60°C to +125°C using a dry ice chamber for the low temperature and a Blue-M low temperature furnace for the temperatures above 25°C. Resistance as a function of power dissipation was evaluated from 10 $\mu W/inch^2$ to 3 $W/inch^2$. The test schematic is shown in Figure 6. Currents and voltages supplied by both meters used were checked against the power dissipation data to insure that the meters were operating in the linear region of the pastes' characteristics. Room temperature storage for 336 hours was also evaluated.

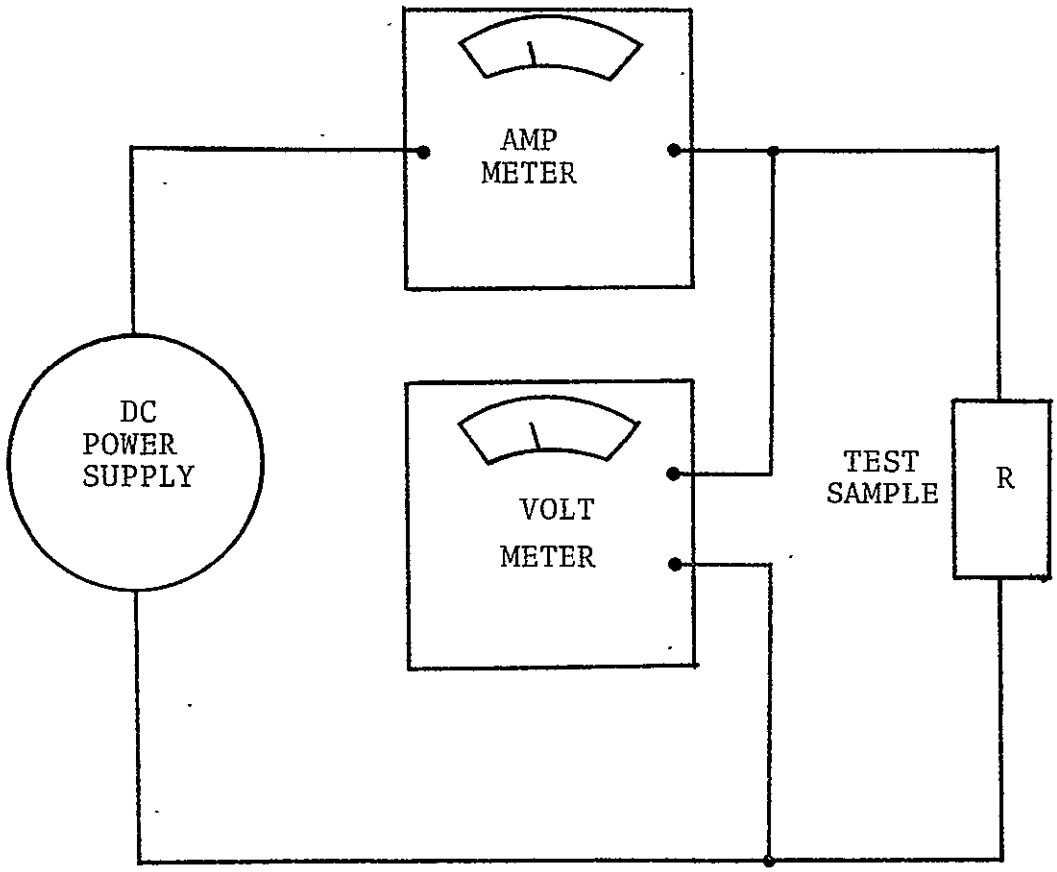

Figure 6. VCR Test Schematic.

CHAPTER IV

EXPERIMENTAL RESULTS

Glass particle size, composition and amount of O.V.,. storage time and amount of thinners used, affected the printability. Average particle sizes of one to three microns yielded optimum printability. Particle size as large as thirty-seven microns were tested, but the pastes made with smaller frit resulted in better prints as shown by Figure 7. Pastes made with the organic vehicle of 20.0 grams of ethyl cellulose per liter of alpha terpineol resulted in the optimum uniformity in the final print. Pastes with 2.5 - 3.0 grams of glass frit per milliliter of O.V. resulted in optimum printability and visual resistor quality.

Relative adhesive quality of the as-fired paste was a function of composition, peak firing temperature and atmosphere. Adhesion is summarized in Table 3. Paste A had the best overall bonding qualities. Generally, the resistors fired in air had the best resistor bond-to-substrate properties.

Resistors fired in air had resistances of 10^{11} to 10^{12} ohms/square, however, resistors fired under hydrogen ranged from 5 Mohms/square to 10 ohms/square. Resistance

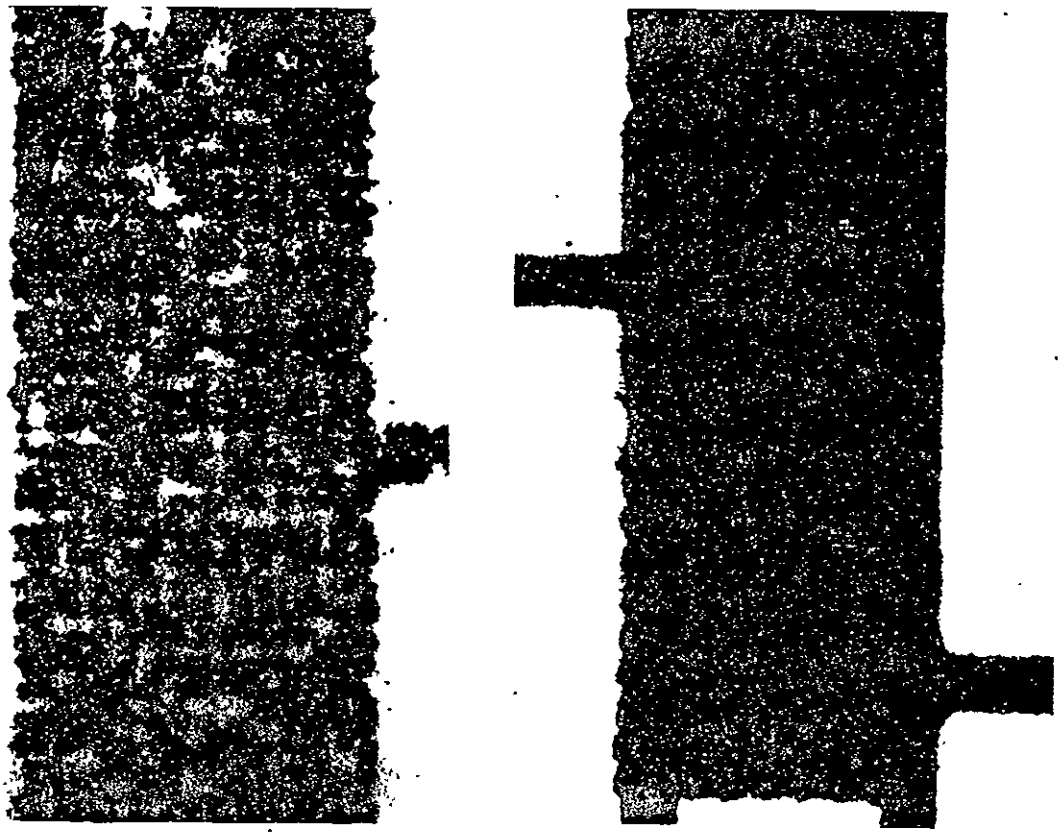

(A) 37 Micron Paste (B) 3 Micron Paste

Figure 7. Backlighted Photographs of Thick Film Prints.

56

Table 3.* Relative Adhesion as Related to Firing Condition

Paste	OXIDIZING ATMOSPHERE			
	600°C	750°C	850°C	920°C
A	G	P	P	-
B	P	-	P	-
C	P	-	-	G

Paste	REDUCING ATMOSPHERE			
	600°C	670°C	850°C	450°C
A	P	F	G	P
B	P	F	F	P
C	P	P	P	P

* G - Good
F - Fair
P - Poor

decreased with increasing iron content and peak temperature had the least effect on the highest iron oxide content paste. Table 4 summarizes resistance as a function of composition and peak firing temperature.

Table 5 summarizes the 336 hour room temperature storage. An average change in resistance of 308 percent indicates the need for some conformal coating, protection or change in composition to eliminate the large drift.

Temperature coefficient of resistance was evaluated from -60°C to +125°C and the data is summarized in Figure 8. Effect of temperature on resistance decreased with increasing iron content.

Voltage coefficient of resistance was evaluated in a power dissipation range from 10 microwatts to 3 watts per square inch. Percent change in resistance versus power dissipation is plotted in Figure 9. Change in resistance decreased with increasing iron content.

Table 4.* Resistance as Related to Reducing Atmosphere Firing

Paste	670°C	850°C
A	5 Mohms	5 Kohms
B	75 ohms	80 ohms
C	200 ohms	10 ohms

* All resistors fired in air R = 10^{11} - 10^{12} ohms.

Table 5. 336 Hour Room Temperature Storage Data

P/N	Resistance Kohms		
	Initial	Final	Percent Change
1	26.7	113.2	324
2	20.7	92.8	348
3	39.1	153.8	293
4	33.6	146.5	336
5	12.6	50.8	303
6	15.8	65.4	314
7	20.4	90.0	341
8	19.3	79.8	313
9	4515.0	7530.0	67
10	30.8	133.1	332
11	66.1	289.8	338
12	54.0	212.2	293
13	21.4	84.0	293
14	25.0	105.3	321
15	44.1	205.0	365
16	29.2	129.9	345
			308 AVE

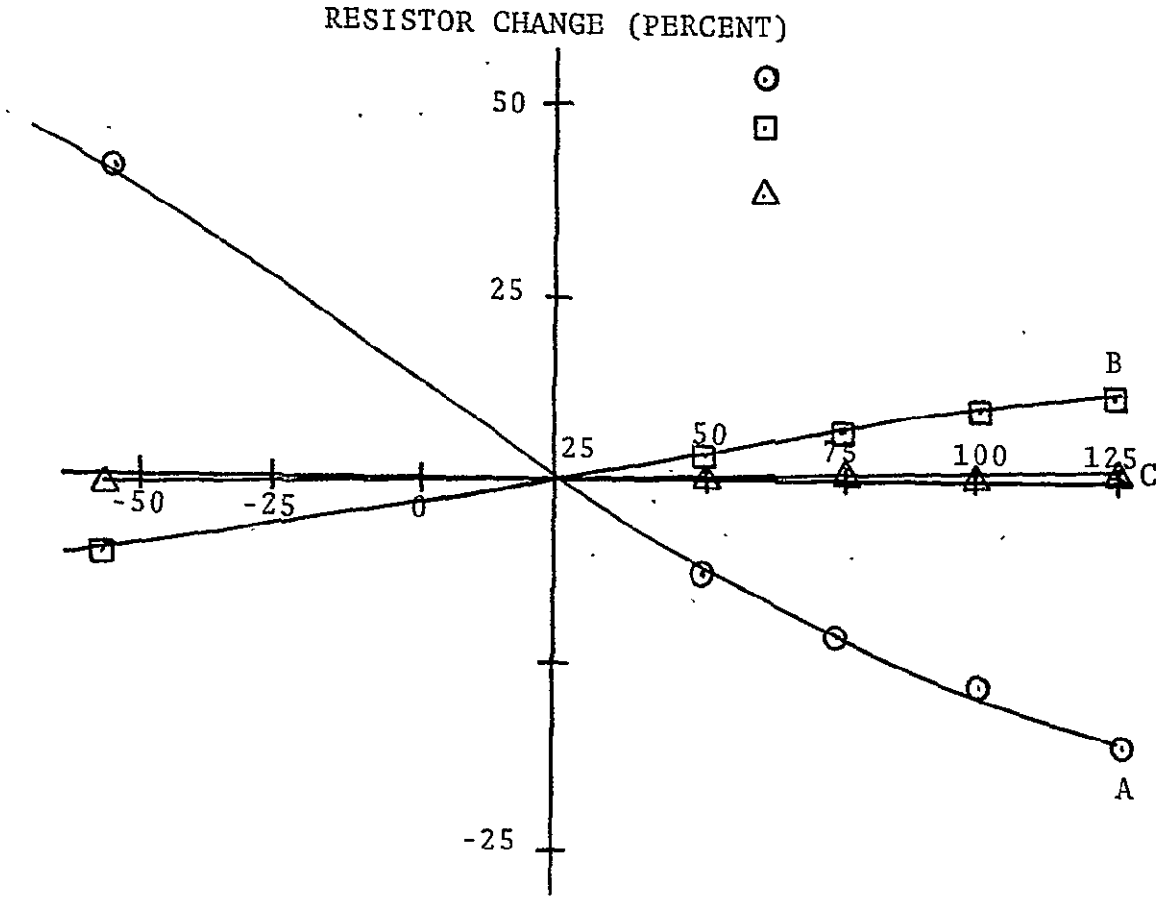

Figure 8 . Resistance as a Function of Temperature for the Three Pastes Examined.

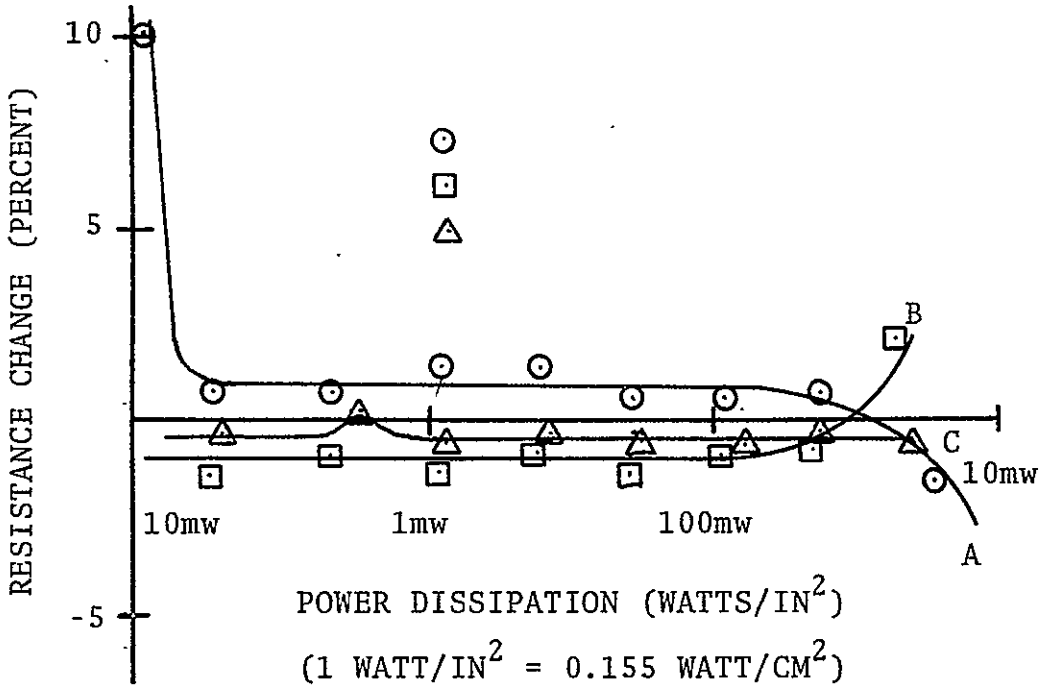

Figure 9. Resistance Change as a Function of Power Dissipation.

CHAPTER V

DISCUSSION OF RESULTS

Rheology

Glass particle size, composition and amount of O.V., storage time and amount of thinners used affected the rheology. Rheology techniques were discussed in the theory section and a "good print" was described as a continuous print where the paste viscosity allowed flow that would eliminate the rough surface inherent to the screen printing process, but now flowing enough to alter resistor dimensions or reduce line resolution.

Particle size used varied from one to thirty-seven microns, limited on the upper bound by the screen mesh. As the particle size approached the screen mesh limits, the surface of the printed resistor became discontinuous and the amount of paste transferred to the substrate was reduced. The larger particle size limited the amount of material passed through the screen which caused the thin appearance of the prints. Figure 7 shows a back lighted photograph of a region printed with the largest and smallest particle size. Smaller particle sizes increased the general quality of the resistor and ease of printing. Optimum results were attained with an average particle size

of one to three microns and an upper bound of seven microns. Samples of the frit were measured with the scanning electron microscope to determine the average particle size. Increasing grinding times made it impractical to prepare particle sizes smaller than one micron.

The organic vehicle was ethyl cellulose dissolved in alpha terpineol in two compositions, 20.0 and 26.8 grams of ethyl cellulose per liter of alpha terpineol. Greater ease of printability and more uniform resistors were produced from the lower ethyl cellulose O.V. The 26.8 grams per liter O.V. paste passed through the screen with greater difficulty and tended to polymerize the paste. The polymerized paste was pulled back through the screen leaving regions of the substrate not printed.

The quality of the resistors was affected by the amount of O.V. used in the paste. Grainy, hard to print paste resulted if too little O.V. was used and excessive O.V. resulted in thin resistors and resolution loss if the thin paste ran. Pastes with 2.5-3.0 grams of glass frit per milliliter of O.V. resulted in optimum printability and visual resistor quality. After three to four weeks of paste storage, thinners were often used to readjust the paste viscosity. Thinners used as needed were diethylene glycol monobutyl ether and diethylene glycol monoethyl ether.

Firing Characteristics

Firing characteristics of the pastes were studied by varying peak firing temperature and atmosphere and are summarized in Tables 3 and 4. Peak firing temperatures ranged from 600°C, which is near the softening point of the glass, to 950°C. Generally, the resistors fired in air had better resistor bond-to-substrate properties. The two component pastes (frit + O.V. only) had best adhesion results with a peak firing temperature of 600°C held for thirteen minutes and cooled to room temperature in eight minutes. Paste B did not have good adherence for either profile used. Paste C (Fe powder added) had maximum adherence for the profile with peak temperature of 920°C. As-fired prints were not always glassy in appearance. In the maximum adherence form paste A was glassy in appearance, but paste C was not.

Resistors fired in air had resistances of 10^{11} to 10^{12} ohms/square, however, resistors fired under hydrogen ranged from 5 Mohms/square to 10 ohms/square. The effect of atmosphere change varied with the iron content. Change in peak firing temperature had little effect on paste B, changing it only 0.67%, but pastes A and C changed from 5 Mohms to 5 Kohms and 200 ohms to 10 ohms, respectively. The controlling factors in the firing process were peak temperature, exposure time to peak temperature and exposure time

to reducing. An even flow rate of hydrogen was required for optimum furnace operation, but the actual flow rate did not appear to be critical in controlling the final resistor values.

Electrical Characteristics

Resistance decreased with increasing iron content with the 70 atomic percent iron paste near 10 ohms/square, the 70 atomic percent iron oxide paste near 100 ohms/square and the 40 atomic percent iron oxide paste near 5 Kohms/square. Room temperature storage was evaluated for 336 hours and the data is summarized in Table 5. Changing oxidation states of the iron in the resistors is the most probable cause of the drift during storage although, this drift was not apparent in the thermal or voltage coefficient tests. Storage drift may be reduced or eliminated by the use of conformal coating to protect the resistor.

Conductivity in the pastes appeared to be an exponential function of activation energy and temperature: $\exp(Q/KT)$, where K is Planc's constant. The activation energy was extracted from the resistance versus temperature data and compared with other studies to evaluate the conduction process.

Paste A shows a negative TCR, which is similar to the bulk glass properties reported by Vaughan[29] but, the activation energy for conduction is significantly less.

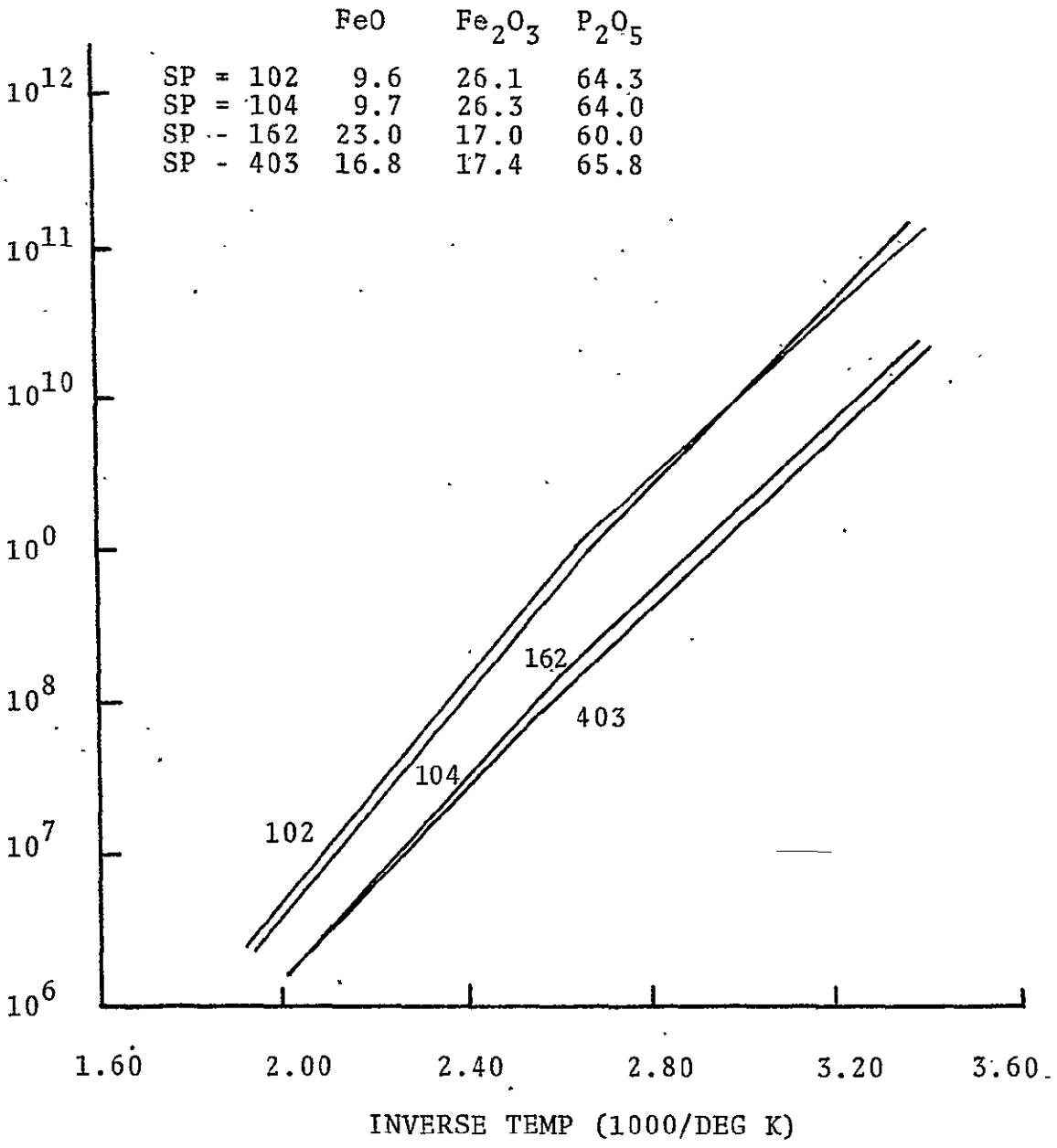

Figure 10. Log_{10} Resistivity vs. 1000/T for Specimens 102, 104, 162 and 403.[30]

Figure 10 is a reprint from Vaughan and Kinser showing resistivity versus inverse temperature from which activation energies were extracted.[31] The activation energy was reported at 20°C and 200°C as being 0.537 eV and 0.631eV, respectively. The activation energy extracted for paste A is 0.034eV, which is in excess of an order of magnitude lower than that of the bulk glass. J. P. Sucket[32] has reported on conductivity in wüstite and from his plot on conductivity versus inverse temperature, reproduced in Figure 11, he extracted an activation energy of 0.067eV. The conductivity of paste A appears to be similar to the conductivity of wüstite and not similar to the bulk glass.

Paste B and C have a positive TCR similar to metallic conduction. Paste C, the highest iron content paste, had the lowest TCR which was, in fact, nearly temperature independent, changing only ± 1% over the range tested.

Voltage and current data taken from the VCR test is replotted in Figure 12. Nonlinearity of the voltage current relationship indicated a non-negligible voltage coefficient. The voltage versus current plots are linear, therefore, the slopes which are the respective resistances, are constant and the resistors are ohmic throughout the region tested.

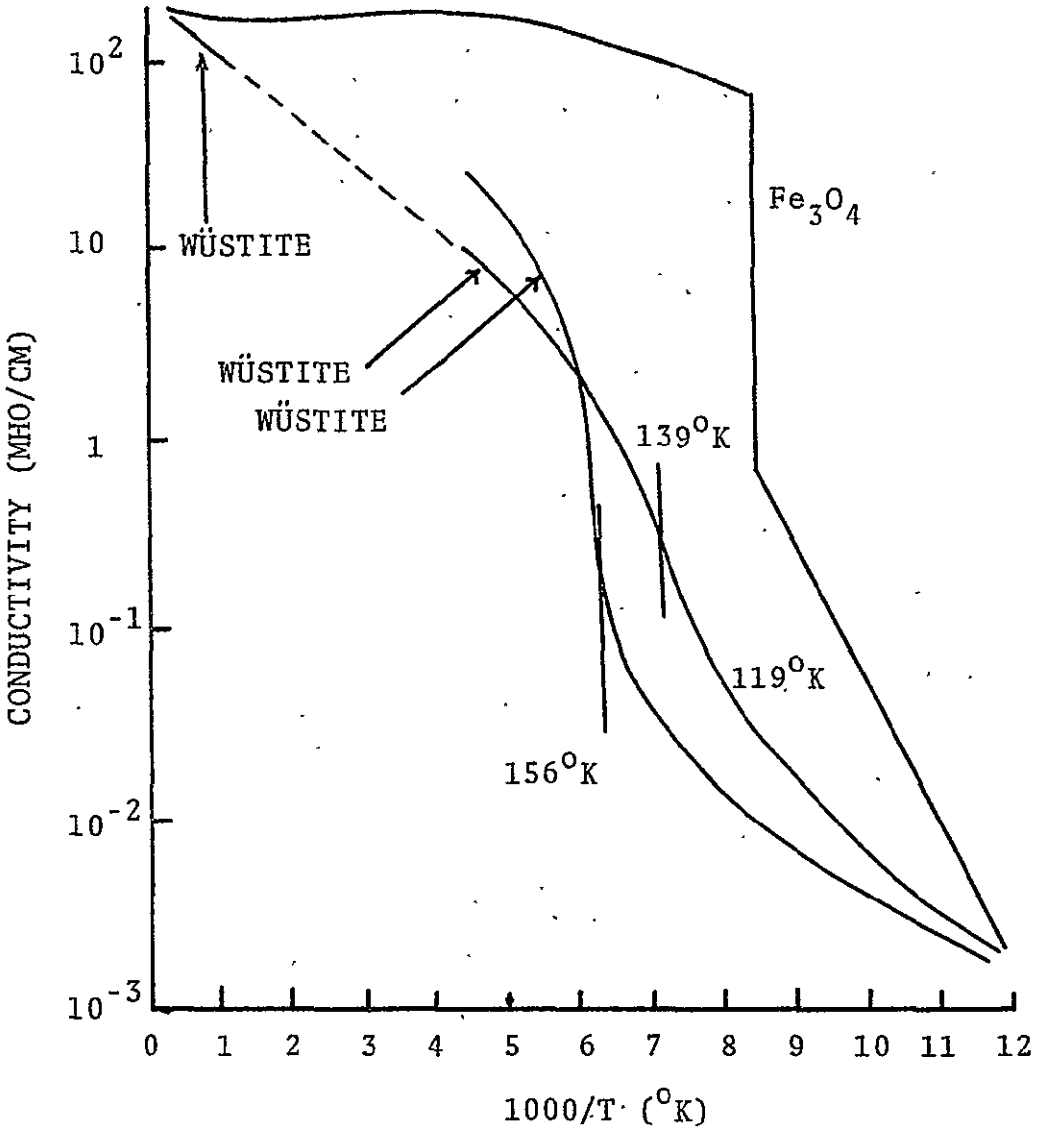

Figure 11. Logarithmic Variation in the Conductivity of FeO in Terms of the Temperature Reciprocal.[33]

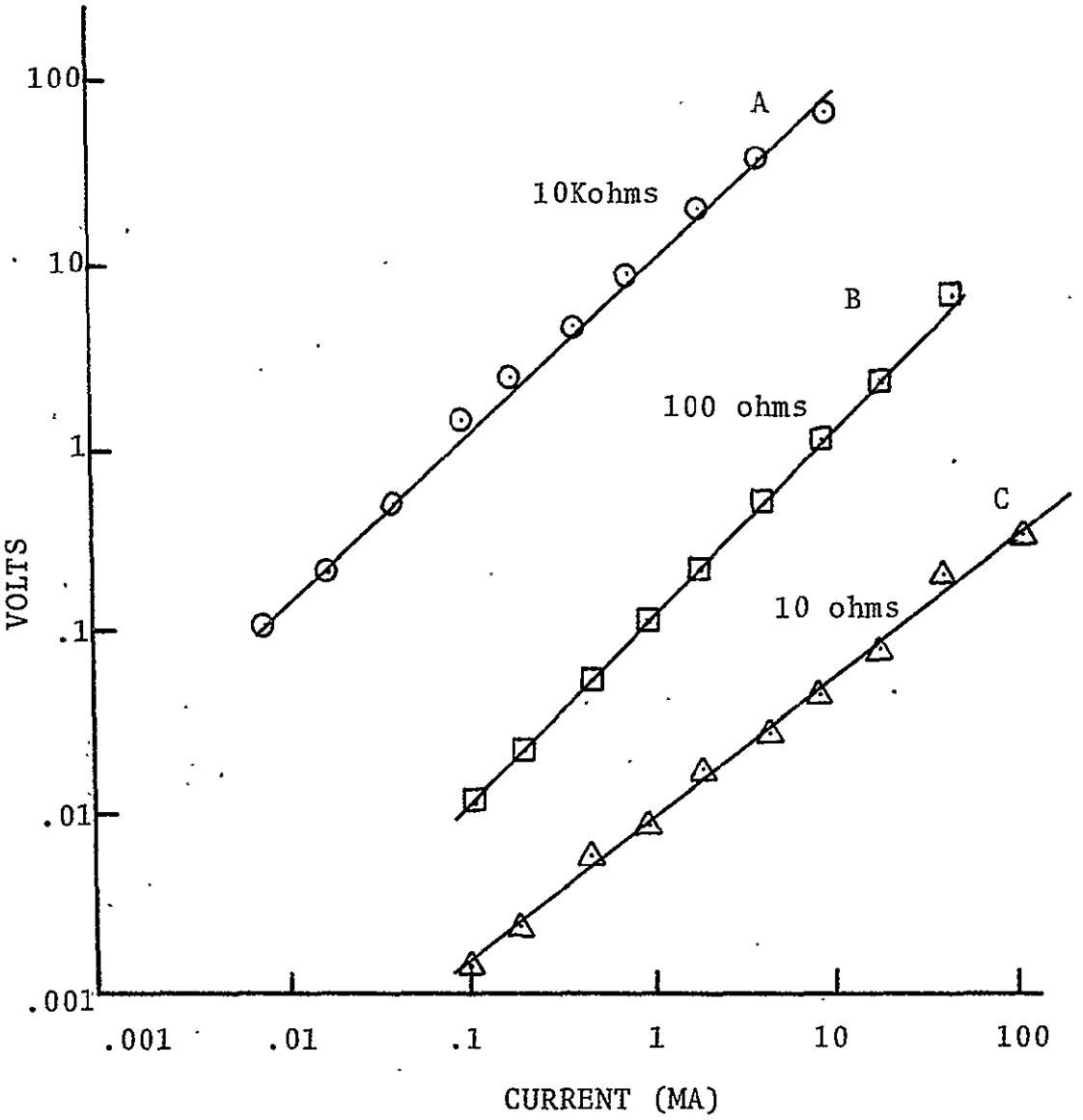

Figure 12. Voltage Versus Current Plot for Pastes A, B. and C.

CHAPTER VI

CONCLUSIONS

Thick film resistors have been developed by grinding samples of the iron phosphate glass system and mixing the frit with an organic vehicle of alpha terpineol and ethyl cellulose. Optimum rheological characteristics were attained by controlling the frit size and the paste mixture ratios. Electrical characteristics were correlated to composition and firing conditions through temperature and voltage coefficient of resistance tests.

Conclusions derived from these tests are enumerated below:

1. Thick film resistors have been successfully prepared from samples of the iron phosphate glass system.

2. Printability was optimized with an average particle size of one to three microns and an upper bound of seven microns. An organic vehicle consisting of 20.0 grams of dry ethyl cellulose dissolved in a liter of alpha terpineol produced optimim printability with 2.5-3.0 grams of glass frit mixed with one milliliter of organic vehicle.

3. Resistance values of an iron phosphate glass thick film system are dependent on composition. Present work indicates that the resistance is inversely proportional to the iron content.

4. Resistor stability of an iron phosphate glass thick film system is dependent on composition. The present work indicates that the higher iron content pastes are the most stable.

5. Resistor value in an iron phosphate glass thick film system is dependent on the firing conditions. The present work indicates that these thick film pastes should be fired under a hydrogen atmosphere with a peak temperature of 850°C.

Notes on Future Research

Although these efforts have successfully produced a thick film resistor paste, a commercially practical system was not developed. A belt furnace with atmosphere control capability would enable a more in-depth correlation of firing conditions and electrical characteristics of the paste. More accurate control of the time/temperature profile during firing could also be used to improve the mechanical strength of the system. Conduction in the iron phosphate system could be better understood through the microstructure of the as-fired resistors. X-ray techniques could be developed to determine the crystalline structures in the resistors. The effect of relative concentrations of Fe^{2+} and Fe^{3+} ions on conduction could be studied with titration techniques.

Several transition metal oxides form glasses with P_2O_5 and could be studied as a possible thick film resistor material. Candidates for this research should include copper phosphate, vanadium phosphate, and titanium phosphate glasses.

LIST OF REFERENCES

1. The Thick Film Microcircuit Handbook, E. I. DuPont DeNemours & Company (Inc.), Photo Products Department Electronic Materials Division, pp. 2.2.1.

2. Ibid.

3. J. M. Robertson, Transition Metal Oxide Glass Thick Film Feasibility Study, School of Engineering Science (Electrical Eng.), University of Edinburgh, March, 1974.

4. J. G. Vaughan and D. L. Kinser, "The Electrical Resistivity Surface for $FeO-Fe_2O_3-P_2O_5$ Glasses," J. Amer. Cer. Soc., 58 (79) 326-329.

5. V. M. Shukla, "Computer Applications to the Hybrid Microelectronic Circuit Design," 1972 International Microelectronics Symposium, pp. 2-B-5-1-8.

6. V. Sookikian, "In-House Artwork and Screen Fabrication for Prototype Thick Film Circuitry," Solid State Technology, June, 1972, pp. 42-47.

7. S. V. Caruso, Interview, NASA/MSFC, Technology Division.

8. R. W. Atkinson, "Squeegee Pressure and Thick Film Resistor Fabrication," Solid State Technology, May, 1971, pp. 51-54, 63.

9. R. A. Vogal, "Fine Line Printing for Consumer Electronics," Solid State Technology, May, 1972, pp. 51-54.

10. Ibid. pp. 51-54.

11. J. R. Larry, "Influence of Surface Energies on Line Resolution in Screen Printing," Solid State Technology, June, 1972, pp. 48-51, 58.

12. Loc. cit. pp. 2.2.1.

13. Vaughan and Kinser

14. A. W. Dozier, L. K. Wilson, E. J. Friebele and D. L. Kinser, "Correlation of Structure and Electrical Properties of $55FeO-45P_2O_5$ Glass," J. Amer. Cer. Soc., 55 (7) 373-377.

74

15. Robertson

16. Ibid. pp. 4

17. Ibid. pp. 5

18. Ibid. pp. 7

19. Robertson

20. Ibid.

21. Ibid. pp. 7

22. Dozier et al.

23. Dozier

24. E. J. Friebele, L. K. Wilson, A. W. Dozier and D. L. Kinser, "Antiferromagnetism in an Oxide Semiconducting Glass," Phys. Stat. Sol. 45 (b) 323-331 (1971).

25. A. M. Bishay and L. Maker, "Role of Iron in Calcium Phosphate Glasses," J. Amer. Cer. Soc. 52 (11) 605-609 (1969).

26. Vaughan and Kinser

27. Robertson, pp. 9

28. J. G. Vaughan, "Correlations Between Structure and Electrical Properties in Iron Phosphate Glasses," M. S. Thesis, Vanderbilt University, 1974.

29. Vaughan and Kinser

30. Ibid.

31. Ibid.

32. J. P. Sucket, Crystal Chemistry and Semiconduction in Transition Metal Binary Compounds, Academic Press, New York, 1971, pp. 167-170.

33. Ibid.

75

BEST SELLERS

FROM NATIONAL TECHNICAL INFORMATION SERVICE

NTIS

Fire Safety Aboard LNG Vessels
ADA-030 619/PAT 295 p. PC$9.25/MF$3.00

Solar Energy Heat Pump Systems for Heating and Cooling Buildings, Proceedings of a Workshop Conducted by the Pennsylvania State University College of Engineering June 12-14, 1975
COO-2560-1/PAT 240 p. PC$8.00/MF$3.00

Data Encryption Standard. Category: ADP Operations. Subcategory: Computer Security
FIPSPUB 46/PAT 20 p. PC$3.50/MF$3.00

Criteria for Evaluation of the Health Aspects of Using Flavoring Substances as Food Ingredients
PB-257 184/PAT 109 p. PC$5.50/MF$3.00

Fundamental Aspects of Nuclear Reactor Fuel Elements
TID-26711-P1/PAT 625 p. PC$16.25/MF$3.00

Patrol Force Allocation for Law Enforcement: An Introductory Planning Guide
N76-24084/PAT 51 p. PC$4.50/MF$3.00

FAA Statistical Handbook of Aviation. Calendar Year 1975
ADA-033 210/PAT 158 p. PC$6.75/MF$3.00

Neutron Cross Sections. Volume II
BNL-325ED3V2/PAT 519 p. PC$12.75/MF$3.00

A Study of Hospital Patient Injury Prevention Programs
PB-260 733/PAT 200 p. PC$7.50/MF$3.00

NIOSH Analytical Methods for Set N
PB-258 433/PAT 56 p. PC$4.50/MF$3.00

Ocean Carrier Service Image and Marketing Practices
PB-261 181/PAT 150 p. PC$6.00/MF$3.00

Manual of Methods for Chemical Analysis of Water and Wastes
PB-259 973/PAT 317 p. PC$9.75/MF$3.00

HOW TO ORDER

When you indicate the method of payment, please note if a purchase order is not accompanied by payment, you will be billed an additional $5.00 *ship and bill* charge. And please include the card expiration date when using American Express.

Normal delivery time takes three to five weeks. It is vital that you order by number or your order will be manually filled, insuring a delay. You can opt for *airmail delivery* for $2.00 North American continent; $3.00 outside North American continent charge per item. Just check the *Airmail Service* box. If you're really pressed for time, call the NTIS Rush Handling Service (703) 557-4700. For a $10.00 charge per item, your order will be airmailed within 48 hours. Or, you can pick up your order in the Washington Information Center & Bookstore or at our Springfield Operations Center within 24 hours for a $6.00 per item charge.

You may also place your order by telephone or if you have an NTIS Deposit Account or an American Express card order through TELEX. The order desk number is (703) 557-4650 and the TELEX number is 89-9405.

Thank you for your interest in NTIS. We appreciate your order.

METHOD OF PAYMENT

- ☐ Charge my NTIS deposit account no. _____
- ☐ Purchase order no. _____
- ☐ Check enclosed for $_____
- ☐ Bill me. Add $5.00 per order and sign below. (Not available outside North American continent.)
- ☐ Charge to my American Express Card account number

Card expiration date _____

Signature _____

☐ Airmail Services requested

NAME _____

ADDRESS _____

CITY, STATE, ZIP _____

Item Number	Quantity		Unit Price*	Total Price*
	Paper Copy (PC)	Microfiche (MF)		

All prices subject to change. The prices above are accurate as of 6/77

Foreign Prices on Request.

Sub Total	
Additional Charge	
Enter Grand Total	

Clip and mail to

NTIS

National Technical Information Service
U.S. DEPARTMENT OF COMMERCE
Springfield, Va. 22161
(703) 557-4650 TELEX 89-9405